

CAVITATION STUDIES IN AXIAL INDUCERS

Thesis by

Henry John Nawoj

Lieutenant, U. S. Navy

In Partial Fulfillment of the Requirements

For the Degree of

Aeronautical Engineer

California Institute of Technology

Pasadena, California

1956

ACKNOWLEDGEMENTS

The writer would like to express his deepest appreciation to Dr. A. J. Acosta who initiated and guided this work.

The writer is also indebted to Mr. R. D. Bowerman for his assistance and advice.

Acknowledgement is also made to the staff of the Hydrodynamics Laboratory of the California Institute of Technology for assistance with the experimental work.

ABSTRACT

Cavitation development was investigated in axial inducers from inception to impeller breakdown using the conventional hydraulic parameters and direct visual observation. Five distinct regimes of cavitation development were observed, and the noise and vibration associated with cavitating pumps was found to occur principally in only one regime of cavitation development. Cavitation in a highly cavitating inducer was found to be adequately modeled using the cavitation similarity number introduced by Prandtl. A simple model is presented for impeller breakdown and experimental data indicate that the general requirements for impeller breakdown given by the model are exhibited in the experimental impellers. A modification to the cavitation number is suggested to accommodate the effusion of dissolved gases from the working fluid into the cavities.

TABLE OF CONTENTS

PART	TITLE	PAGE
	ACKNOWLEDGEMENTS	
	ABSTRACT	
	TABLE OF CONTENTS	
I.	INTRODUCTION	1
II.	PROPOSED INVESTIGATION	6
III.	EXPERIMENTAL APPARATUS AND EXPERI- MENTS CONDUCTED	
	A. Facility Description	7
	B. Impeller Selection, Design, and Construction	9
	C. Inducer Drive and Speed Regulation	11
	D. Hydraulic Instrumentation	14
	E. Photographic and Lighting Facilities	16
	F. Preparation of the Facility for Experimental Runs	16
	G. Non-cavitating Studies	17
	H. Cavitating Studies	18
	I. Estimation of Errors	19
IV.	THEORETICAL REMARKS	
	A. Cavitation Failure or Breakdown	22
	B. Gas Effusion into a Cavity Bubble	26
V.	RESULTS AND DISCUSSION	
	A. Non-cavitating Performance	28
	B. Cavitating Studies	
	1. Performance	29
	2. Photographic and Visual Studies	31
	3. Tip Clearance Effects	34

TABLE OF CONTENTS (Cont'd)

PART	TITLE	PAGE
	4. Impeller Breakdown	36
	5. Cavitation Scaling	37
VI.	CONCLUSIONS	39
	REFERENCES	41
	APPENDIX I - NOTATION	43
	APPENDIX II - DETERMINATION OF NON-DIMENSIONLESS PARAMETERS	45
	FIGURES	50-81

I. INTRODUCTION

The development of the liquid rocket motor into a practicable source of thrust for missiles and the accompanying use of exotic liquid fuels and oxidizers having thermodynamic properties vastly different from the normal liquids with which pump designers have had to contend has generated a much more stringent set of design requirements for the pump designer to meet. The prime design requirement that must be met is the weight and space reduction of the entire pumping machinery package by orders of magnitude without any reduction of the flow rate or head outputs.

The requirement forces the selection of turbomachinery as the only pumping machinery capable of delivering the large volume of fluid required with the desired head output yet remaining within the limitations of the weight and space requirements. In addition, the use of the impulse turbine as the driving element demands that the pump machinery operate at high rotative speeds to eliminate or reduce heavy gear trains between the turbine and the pump (Ref. 1 and Ref. 2). These high rotative speeds, coupled with a head rise in the order of twenty atmospheres, require extreme local fluid velocities with respect to the impeller blade. From Bernoulli's Law, the static pressure of the fluid must be reduced, and the reduction is generally to such a degree that the static pressure becomes less than the vapor pressure of fluid. In this state, the fluid is thermodynamically unstable, and the condition is relieved by the formation of vapor bubbles on the impeller blading. This phenomenon, known as cavitation, has, as an immediate consequence, the reduction of through flow area within the pump, causing

a decrease in the volume output of the unit.

A further consequence of the cavitating flow is impeller damage caused by the collapse of the vapor bubbles. Cavity collapse is usually rapid, permitting the liquid boundary of the cavity to strike the impeller surface with a high velocity. The resultant impact stresses, though lower than the failure stress of the materials commonly used in impeller construction, occur repeatedly, and may rapidly reach the fatigue limit of the material (Ref. 3).

To aggravate cavitation further, the missile utilizing rocket propulsion operates most efficiently in the outer reaches of the atmosphere where atmospheric pressure is negligible, further reducing the static pressure available at the pump entry.

Pumps operating in a highly cavitating flow field are not peculiar to rocket engines; other typical applications are the condensate pumps in steam power plants and aircraft fuel pumps. The problems encountered have been solved by extreme over-design of the pumps. In a missile, however, the penalty that must be paid in loss of missile performance for the decrease in loading density of the missile is too severe to permit extensive over-design of any component (Ref. 3).

One solution of the cavitation problem in missile fuel pump system has been the conversion of the fuel and oxidizer storage tanks to pressure vessels, and the use of an inert gas to pressurize the tanks to maintain the local static pressure at the impeller above the vapor pressure of the fluid (Ref. 2). This solution eliminates the problems caused by operation outside

the earth's atmosphere; however, the decrease in loading density of the missile caused by the increased weight of the fuel storage tanks and the inert gas does not make this generally the optimum solution for rocket motors producing large thrusts for a long period of time.

Another solution is the use of a booster pump or inducer capable of operating in a highly cavitating flow field to supercharge the inlet of the main pump sufficiently to eliminate cavitation. The inducer may be mounted integrally with the main pump (Ref. 2), or may be a separate unit in the flow system.

The proper design of such an inducer is dependent upon a knowledge of the internal flow in the inducer when operating in a cavitating regime. This information is not yet generally available. Thus, it is of some importance to obtain knowledge of internal flow in hydrodynamic machinery when cavitation is present and to interpret this information in terms of the performance parameters of the machinery.

The performance of hydrodynamic machinery is usually given in terms of dimensionless head, flow and torque coefficients (Appendices I and II). From the principles of dynamic and kinematic similarity, the non-cavitating performance of geometrically similar machines will be the same at corresponding flow rate coefficients if the Reynolds number is the same; however, significant changes may occur during cavitation, since the cavities distort the flow geometry, and in so doing, alter the performance.

The mechanics of cavity formations is very complex; however, if the Reynolds number is not too low, it has been found that the extent and effect of cavitation is governed by a pressure coefficient introduced by Prandtl. This coefficient is called the cavitation number, and is defined as the difference between the undisturbed stream pressure and cavity pressure divided by the free stream dynamic pressure.

In many experiments on hydrofoils and pumps, the performance at a given angle of attack or flow coefficient has been found to be only a function of the cavitation number (Refs. 4, 5, 6, 7). In all these experiments, water was the working fluid, and, since the ratio of the vapor to liquid density is negligible, the cavity pressure was considered constant. However, the cavity pressure is usually unknown, and is frequently assumed to be the vapor pressure of the fluid at the liquid bulk temperature. This assumption can introduce considerable error into "cavitation number" scaling.

In the hydraulic machinery literature, the cavity pressure is assumed to be the vapor pressure; two additional similarity parameters (related to each other and to the cavitation number) are used in the interpretation of cavitation tests. These are the Thoma cavitation parameter (the ratio of the total inlet head minus the vapor pressure to the non-cavitating impeller head), and the "suction specific speed" introduced by Bergernon (Appendix I).

Some results (Ref. 4) have shown that dynamic flow similarity is adequately maintained if either the cavitation number, based on the liquid vapor pressure, or the above parameters are scaled. However, these tests were conducted over a small range of rather high cavitation number and throughout a limited speed range.

Now it seems clear that the effects of air diffusion into the cavity and the evaporation of vapor into the cavity and the subsequent entrainment of the cavity gases into the fluid stream are important factors in determining the cavity pressure. Thus, the adequacy of the usually used cavitation similarity parameters is open to question, particularly for those situations in which the free stream pressure is only slightly above the vapor pressure.

In the sections that follow, the objectives of the present work will be outlined, and the experimental program described. A simple model for cavitation "breakdown" is put forward and is compared with the results of the experiments.

II. PROPOSED INVESTIGATION

From the foregoing discussion, it is clear that pumps are and will be operated under conditions of extreme cavitation. The ultimate aim of any investigation of this problem is to provide means of designing pumps to operate successfully under such conditions, and further, to give criteria for the "best" type of pump to be used in extreme cavitation.

Such a program is, of course, much too ambitious to be realized quickly. As a first step, it is necessary to have as complete knowledge of the flow field as possible. Consequently, the major objective of this work is to describe the development of cavitation in an axial flow inducer from its inception point to cavitation breakdown of the impeller for the range of operating flow rates. Insofar as possible, the effect of cavitation on performance will be correlated with the appearance of the internal flow field so that the significant regimes of cavitation can be ascertained.

It is also expected that cavitation will occur under conditions where similarity will not be given by the cavitation number (or other derived parameters) when based upon the liquid vapor pressure. An additional objective, therefore, is to determine the validity of the parameters within the scope of the experimental facility.

Since optimum pump design requires a knowledge of impeller breakdown conditions, a simple model for breakdown is proposed and experimental verification of the model will be attempted.

III. EXPERIMENTAL APPARATUS AND EXPERIMENTS CONDUCTED

A. Facility Description:

An axial flow pump facility was designed and built at the Hydrodynamics Laboratory at the California Institute of Technology for the purpose of making cavitation studies of inducer-type pumps operating at low suction pressures or low cavitation numbers. The apparatus permits measurement of the overall inducer performance as well as visual observation of the flow.

The facility is a closed hydraulic circuit consisting of storage tank of 60 gallon capacity, the test section, a return system and appropriate hydraulic and electrical instrumentation. Figure 1 shows the general features of the system.

The top of the storage tank is used as a mount for the axial inducer. An entrance bell is installed in the top of the tank, and provision is made for sealing the lucite bowl used as the impeller casing to the storage tank.

The impeller casing is manufactured from a block of lucite bored to the nominal diameter of the impeller. Provisions are made to introduce total head probes upstream and downstream of the impeller and two static pressure taps are placed as far upstream of the impeller as possible. The lower impeller drive shaft bearing is mounted at the lower end of the impeller casing, and is installed in a hemispherical fairing. The fairing is supported from the casing wall by four sharp-edged, thin-sectioned, streamlined struts designed to prevent cavity formation on the struts during operation of the inducer.

The impeller shaft was manufactured from 18-8 stainless steel, and was designed to permit expeditious interchange of test impellers yet retain dimensional constancy in impeller location.

Mounted atop the impeller casing is a volute diffuser adapted from a commercial fuel pump manufactured by Hydro-Aire, Inc. The carbon ring seal and thrust bearing specified in the original assembly were retained and used for the impeller drive shaft. Additional diffusion is provided by a diverging conduit which expands the flow from the internal diameter of the volute discharge nozzle to the internal diameter of the return plumbing. The return plumbing is manufactured from 2 inch steel pipe.

A propeller type flow meter manufactured by the Waugh Engineering Co. is installed in the return plumbing and discharges to the main storage tank through a shutoff valve. In addition, a bypass line is provided with a commercial centrifugal pump having a nominal capacity of 90 gpm installed to act as a service pump for the inducer circuit. Valving is arranged to permit utilization of the service pump output from zero flow to maximum flow throughout the entire circuit. Figure 2 gives the arrangement of the flow circuit schematically.

Inasmuch as it was desired to operate the system at pressures approaching the vapor pressure of water, an air-water interface was provided by mounting a small reservoir slightly above the entire facility and connecting it with the storage tank. The reservoir was connected to the high vacuum source available at the Hydrodynamics Laboratory. Several bleed points were

established on the top of the storage tank, in the volute housing, and in the return plumbing. After assembly of the inducer, all joints were sealed with commercial sealing compound to provide airtight joints.

A difficulty was encountered during the operation of the first impeller. Solid particles, in suspension in the water, would become impaled on the leading edge of the impeller and modify the cavitation bubble distribution and induce new cavities. An inlet screen was devised and placed over the inlet to the inducer. The size of the screen was sufficiently large that no observable head losses could be measured at the flow rates used in the inducer studies.

B. Impeller Selection, Design, and Construction

Since the use of a highly cavitating impeller probably will be confined initially to axial inducers, the design of the experimental inducer was made to favor operation at low cavitation numbers or high suction specific speeds. General design conditions for an inducer are:

1. have minimum vane thickness to prevent blockage of the cross-sectional area,
2. be reasonably efficient so that not too great a penalty is paid in performance,
3. have a reasonably high solidity, (blade chord divided by peripheral spacing), to avoid strong local underpressures,
4. be relatively easy to fabricate.

These considerations led to the selection of a rigid helix as the basic inducer design. For reasons of mechanical strength

and ease of manufacture, the experimental impellers were made with four blades. The nominal tip radius was 1.000 inches, and the tip blade angle measured with respect to the plane of rotation was 12.05° . The lead for a helix is constant so that the tangent of the blade angle was inversely proportional to the radius. The axial extent of the impellers was constant so that the solidity decreased slightly from root to tip.

High solidity was needed to satisfy another experimental requirement. To assure perfect guidance of a fluid by an impeller theoretically requires an impeller of infinite solidity. Wislicenus gives the head correction factor for an axial impeller having a solidity of 1.67 and a blade angle of 15° as .996 (Ref. 3), and approaches unity as the solidity of the impeller increases. The head correction factor is an empirical constant designed to measure the conformity of a flow to the impeller blading and has a value of one for an impeller of infinite solidity. A tip solidity of 2.5 was chosen arbitrarily to permit consideration of the experimental impellers as ones of infinite solidity, and to avoid the development of strong local underpressures on the impeller.

Impeller tip clearances were determined from the tip clearance parameter λ (tip clearance over maximum blade tip thickness) defined by Rains (Ref. 5). One impeller was manufactured with a $\lambda = .045$; the other, with a $\lambda = .098$, which is the optimum value of the tip clearance parameter to prevent cavitation inception.

Leading edge profiles were arbitrarily selected. The

profiles used were a sharp-edged profile edged symmetrically about the thickness of the blade, and a sharp-edged profile edged perpendicularly to the axis of the impeller. Impeller details are shown in Fig. 4.

The impellers were manufactured from 24 ST aluminum. Because of fabrication difficulties, the radial thickness distribution of the blade section varied continuously, being thinnest at the root and thickest at the tip. After machining and polishing, the impellers were anodized for corrosion protection.

C. Inducer Drive and Speed Regulation

The inducer drive was a double ended $\frac{1}{2}$ h.p. series wound d. c. motor modified for separate field excitation. The no-load rated speed of the motor was 18,000 rpm. The motor was mounted on top of the inducer housing as shown in Fig. 3. On the other end of the motor a selsyn generator was attached through an 8:1 spur gear reduction.

The original intent in the design of the drive system had been to use the dynamometer control system and power supply installed at the Hydrodynamics Laboratory. The power supply uses three phase, 220 volt a. c. for armature power, and variable voltage d. c. for the field supply. The speed regulation of the dynamometers is obtained by control of the d. c. field voltages.

Speed measurement is accomplished in the control unit by comparing the selsyn generator output with the rpm of a constant speed source. Visual and aural indicators are provided to

indicate an "on-speed" or "off-speed" condition. Speed regulation of the drive motor is obtained by using a signal obtained from a differential gear system between the selsyn receiver and the constant speed motor to control the d. c. field voltage available to the drive motor.

The sensitivity of the system can be adjusted to provide indication and correction of rpm variation of the order of 0.1 percent. The speed range available on the speed control mechanism is from 1 to 999 rpm in unit steps. Inasmuch as an 8:1 stepdown gearing is provided from the drive motor of the inducer to the selsyn generator, and a 3:2 reduction is present between the output of the selsyn receiver and the differential mechanism, a total speed reduction of 12:1 exists between the inducer drive motor and the differential mechanism. Thus, the actual speed range available to the drive motor is from 12 to 11,996 rpm in steps of 12 rpm. With the speed control mechanism on maximum sensitivity, the maximum speed variation of the inducer is 6 rpm for operation at 6000 rpm, and 9 rpm for operation at 9000 rpm.

Since it was desired to obtain impeller torque absorption data from the electrical power inputs to the drive motor, certain modifications were necessary to the system described above. The major modification made was to convert the a. c. armature current supply to a d. c. power supply by full wave selenium rectifier circuits inserted in each leg of the armature power circuit.

Initial power calibration of the drive motor was accomplished using the facilities of Motordyne, Inc. of Monrovia,

California because of the lack of high speed dynamometers on the campus of the California Institute of Technology. This necessitated the operation of the motor as a pure series motor during its calibration.

An electrical absorption dynamometer was used as an energy receiver during the calibration runs. Speed control of the motor during the calibration runs was accomplished using stroboscopic light. Calibration runs made included electrical power input to the motor running free over the anticipated operating range, i. e., 6-11,000 rpm, and electrical power input vs. output torque with operating speed as a parameter. The results of the initial calibration are shown in Figs. 5 and 6. Data reduction of the initial power calibration curves was obtained by use of a lineal least squares approximation for each parametric value of rpm.

Attempts were then made to obtain correlation data between the initial calibration of the motor as a series motor and its proposed use at the laboratory facility as a shunt motor. Mathematical techniques could not provide this correlation because of extensive non-linearities that apparently develop in the motor when operating as a separately excited unit.

Experimental correlation was then attempted. In attempting to obtain experimental data for correlation curves, it was observed that, when controlled by the automatic speed controller, the variation of the motor field current permitted excessive armature currents to be drawn by the drive motor.

The use of the automatic speed control was abandoned

and the motor was reconverted to a series wound motor. Speed control was done manually, utilizing, however, the visual indicator system of the automatic speed regulator and the armature power supply as originally designed. To obtain fine control of the input power, a π type resistive network using variable resistors was inserted into the armature circuit.

Electrical input power was determined with commercial voltmeters and ammeters having a guaranteed accuracy of 2 percent at full deflection. Prior to use, the meters were calibrated against a master meter providing an accuracy of $1\frac{1}{2}$ percent at full deflection.

Since it was desired to know the actual torque being delivered to the impeller, further calibration was required with the entire inducer facility assembled, but with a spacer having a diameter equal to the drive shaft diameter substituted for the impeller. The variation of the viscous drag forces on the rotating drive shaft was checked at the flow rates used in the study and found to be essentially zero. The torque absorption by the drive shaft seal as the seal pressure varied was also checked. Fig. 7 gives the torque absorption by the drive shaft seal as the absolute seal pressure varied for two parametric values of rpm.

Impeller torque was determined by converting the input electrical power to an equivalent torque and subtracting from the input torque the seal absorption torque.

D. Hydraulic Instrumentation

The hydraulic instrumentation consisted of the propeller flow meter, two total head probes, and two static piezometer

taps. The flow meter was used in conjunction with a Hewlett-Packard electronic counter. The output signal of the flow meter required electronic amplification to actuate the counter properly. Flow rates were recoded as cycles per second and then converted to cubic feet of flow per second using the meter manufacturer's calibration data.

Total head was measured with simple impact tubes. The design of the total head probes permitted radial surveys of the flow passage to be made. Both total head probes were mounted in the lucite impeller casing; one, mounted on the downstream side of the casing approximately one inch downstream of the trailing edge of the impeller; the other, .50 inches upstream of the leading edge of the impeller. All total head readings were made on mercury-water manometers that could be read to .01 inches.

The absolute pressure existing in the storage tank was measured with a mercury-water manometer measuring the difference in pressure between the tank and the atmosphere. All readings were taken to the nearest .01 inch.

A second flow measuring device was used to check the validity of the propeller flow meter readings. An air water manometer was used to measure the depression of static pressure between the storage tank and the upstream side of the impeller casing. Readings were made to the nearest .001 feet.

All manometer connections were arranged to prevent the formation of vapor cavities in the manometer lines as the pressures in the system were reduced to the minimum values obtainable from the high vacuum source used.

E. Photographic and Lighting Facilities

Still photography was the only photography employed throughout this investigation. A 4 x 5 inch view camera was used, and two Edgerton type flash units having a flash duration in the order of 4 microseconds were employed for cross lighting of the impeller.

Synchronization of the flash units was accomplished by a make-break contactor actuated by a cam on the selsyn generator drive shaft. Phase rotation was provided between the contactor and the cam lobe to permit examination of all blades of the impeller.

Lighting for visual observation was obtained from a strobolux lighting unit synchronized by the same contactor used for the flash units. Occasional difficulty was experienced with the illumination because of the cam design requirements. The actuation time of the contactor was sufficiently long that the opening and closing of the contactor could trigger off successive flashes of the strobolux creating an impression of impeller "bounce". A partial solution was obtained by decreasing the included angle of the cam lobe. The flash units were not affected because of the long recycling time of the capacitors in the flash power supply.

F. Preparation of the Facility for Experimental Runs

Before any data could be obtained from the facility, extensive deaeration of the water in the entire system was undertaken to eliminate, as far as possible, the effects of gas diffusion. Deaeration was accomplished by reducing the absolute pressure within the system as low as possible, operating the inducer at a low speed for a short period of time, and then shutting down the inducer and

waiting for approximately fifteen minutes to allow the gas removed from solution to collect. The system vacuum was then relieved and the air bubbles bled off. The process was repeated until the air content of the water was reduced to the desired level. Because of the limited time available for experimentation, a maximum level of air content was set arbitrarily 3.5 ppm, which was 13.9 percent of saturation air content of water at 20° C.

Air content was measured with the Van Slyke Blood Gas Apparatus (Ref. 9) (Central Scientific Co.). The apparatus determines air content by placing a sample of water under a very low absolute pressure, agitating it for a set period of time with an agitating device, and then comparing the volume of gas evolved from the water with a calibration table. Readings are given as weight of air dissolved per million weights of water.

G. Non-cavitating Studies

A set of non-cavitating performance data was taken for each impeller to provide basic head, flow and efficiency curves for the impellers. In addition, total head surveys were taken upstream and downstream of the impeller to obtain the radial distribution of the flow velocities in the impeller casing at minimum and maximum flow rates studied.

The impeller shaft and casing were tufted to provide an indication of the three-dimensional flows existing within the pump casing. Photographs of the flow patterns were taken over a wide range of flow rates.

H. Cavitating Studies

The studies were limited to a range of flow rates extending from about 40 percent below to 50 percent above the best efficiency flow rate of the impellers. This is considered the range of interest for this impeller design.

Prior to the start of a run, the barometric pressure, air temperature, water temperature and air content of the water were observed and recorded. The inducer was operated for about fifteen minutes to permit warmup and stabilization of the electrical and electronic components.

Following warmup, the inducer was brought to the proper rotative speed and the flow rate desired was established by proper manipulation of the valves in the return plumbing. The downstream total head probe was set for maximum head indication. Data taken were the storage tank static pressure, the downstream total head, and the voltage and amperage applied to the drive motor. Vacuum was applied to the storage tank to reduce the absolute pressure in increments of approximately 2 inches of mercury, the rpm and the flow rate reestablished, and the required readings taken.

The impeller was examined for cavitation using the strobolux light and the visual observation recorded. If significant changes occurred in the cavitation, a photograph was made. The procedure was repeated until: (a) the maximum vacuum available was applied to the storage tank; (b) cavitation became so extensive that it was impossible to maintain control of the inducer, or (c) the flow rate could not be maintained through the inducer.

The inducer could not maintain the required flow rates at the higher flow rate coefficients used in the studies because of the hydraulic losses in the return plumbing. The service pump was used to overcome these losses and permit data to be taken for the inducer. At impeller blade angles of attack approaching 0° , a major limitation of the system became apparent; i. e., the absolute pressure of the storage tank could be reduced only a few inches of mercury before the cavitation in the return plumbing and the service pump became so extensive that the required flow rate could not be maintained.

The propeller flow meter was checked to see if true flow readings were obtained at various cavitation numbers. It was discovered that significant errors were being obtained at moderate values of the cavitation number with a flow rate coefficient of $\phi = 0.16$, and at the very small values of the cavitation number for the lower flow rates. Reruns were made for all points of questionable accuracy using a water-air manometer to measure the static pressure drop between the storage tank and the upstream side of the impeller casing. The flow meter errors were believed caused by the formation of vapor cavities on the propeller of the flow meter.

I. Estimation of Errors

The errors involved in the determination of the calibration curves for the drive motor included: errors in speed determination; errors in the measurement of electrical power; errors in the measurement of torque; and errors introduced by the use of the lineal approximation of the torque-power curves.

The source of maximum error was in the measurement of the electrical power. For low values of input power to the motor the error could rise to $3\frac{1}{2}$ percent. The maximum error in the speed measurement was less than one percent. Torque measurement was accomplished with a weight and pulley system using a null indication, and was believed to be correct to within two percent. The maximum scatter in the lineal approximation of the torque-power curve is in the order of seven percent; which, when the errors possible in the other variables are considered, indicates the approximation to be correct to within two percent.

The errors in impeller torque determination are not amenable to evaluation because of the non-reproducibility of the seal torque absorption data. It is believed that the breakdown and re-assembly of the inducer assembly required to obtain the seal torque absorption data caused different pre-loads on the seal. The variation in impeller torque did not amount to more than five percent at full load conditions.

The errors in the flow measuring apparatus were constant for all flow rates used and had a maximum value of .5 percent.

Some error in the measurement of the total head was generated by fixing the total head probe at the mid-radius of the pump passage, thereby neglecting the radial distribution of head. True total head values could have been obtained by making radial surveys of the fluid passage and weighting the local head readings with the volume flow to obtain a mean value of total head. Since it was desired to determine the deterioration of the total head output for cavitation increase at constant flow rate, it was felt

that this error would not invalidate the results obtained.

The total head measurements were reproducible to within a one percent variation on successive runs at identical flow and cavitation conditions. It was observed that the total head was extremely sensitive to upstream disturbances within the impeller casing. The use of lucite, with its dimensional instability, caused some change in the shape and size of the impeller casing. After five months of operation, variation of the internal diameter of the casing was as high as .25 percent throughout the length of the casing. Eccentricity of the casing was also observed. Total head measurements of similar runs but with a time lag of three months between runs showed variations in total head as high as three percent.

IV. THEORETICAL REMARKS

A. Cavitation Failure or Breakdown

If the inducer is operated at constant speed and flow rate and the cavitation number is gradually reduced, the head and efficiency will commence to fall off. The decrease may be rapid or slow depending upon the flow rate as will be seen later. For any given flow coefficient, however, there will be a cavitation number below which the pump fails to produce positive head. This condition is sometimes called cavitation "breakdown," and the cavitation number, K , corresponding to this condition is called the cavitation breakdown number. This parameter is of some interest, since it represents the extreme cavitation condition that can be attained, and the proximity of the operating point to breakdown is indicative of the margin left in the pump performance. Thus, it would be highly desirable to be able to predict the breakdown state, even if only approximately. Unfortunately, the process of cavitation development over simple bluff bodies or flat plate hydrofoils is complicated and requires fairly involved mathematical analysis, so that no great hope is held out for an accurate treatment of cavitating flow in a three-dimensional pump.

It is possible, however, to estimate some bounds for the breakdown cavitation number if a few simplifying assumptions are made. For example, it is known from free streamline theory that the length of a cavitation bubble on a disc or hydrofoil continuously increases as the cavitation number decreases, and ultimately the cavity becomes infinitely long for zero cavitation number. If

it is assumed that the flow proceeds through the axial inducer at a constant radius, then it can be treated as a two-dimensional problem and the blades of the impeller appear as an infinite, repeating lattice or cascade. When cavitation develops on such a cascade, the cavity length will continuously increase with decreasing cavitation number until eventually the flow consists of infinite constant pressure wakes behind the blades and finite width jets between the blades. The flow picture for a cascade of flat airfoils is shown in Fig. 8. This situation corresponds to the breakdown for the assumptions stated.

It will now be assumed that there is no friction and the motion is irrotational. Since the test inducer is of high solidity (and therefore guides the fluid essentially perfectly), it will also be assumed that the cascade is infinitely long. Thus, the fluid leaving angle will be equal to the blade angle. Since there is no friction, the net force parallel to the flat plate cascade is zero, and application of the momentum equation gives the result: (Ref. 8)

$$\left(\frac{V_2}{V_1} + \frac{V_1}{V_2} \right) \cos \alpha + \left(\frac{V_2}{V_1} - \frac{V_1}{V_2} \right) \sin \alpha \cot \beta_1 = 2 \quad (1)$$

where the notation is taken from Fig. 9.

Bernoulli's equation can also be written with respect to the rotor, i. e.,

$$P_1 + \frac{\rho V_1^2}{2} = P_2 + \frac{\rho V_2^2}{2} \quad (2)$$

so that the cavitation number becomes,

$$K = \left(\frac{V_2}{V_1}\right)^2 - 1 \quad (3)$$

It is anticipated that the values of α and K will both be much less than unity. Equation 1 can then be approximately rewritten as,

$$K = \alpha \phi \quad (4)$$

where $\phi = \tan\beta_1$ is the flow rate coefficient. This result gives a minimum value of the breakdown cavitation number, at least for a cascade.

The foregoing condition is probably too optimistic and effective breakdown should occur sooner. This idea is obtained from an inspection of the velocity diagram in Fig. 8. If there is no cavitation or if the cavity bubble lies entirely within the cascade, the fluid leaving angle is still β_2 , (the chord angle), and from continuity the axial velocity at the end of the blade is equal to the incoming axial velocity. The change in velocity (or angular momentum) in this case is $(\cot\beta_1 - \cot\beta_c)V_1\sin\beta_1$. Now if the cavity is only slightly longer than the blade chord, so that the leaving velocity at the cascade exit will be nearly equal to the velocity along the cavity wall V_2 , the increase in whirl velocity is only $V_1\cos\beta_1 - V_2\cos\beta_2$. For the pump to produce positive head this quantity must be greater than zero, or in the limiting case

$$\frac{V_2}{V_1} = \frac{\cos\beta_1}{\cos\beta_c} \quad (5)$$

V_1 and V_2 are related by the cavitation number, and with the assumption of small K and α , equation 5 can be written as

$$K = 2\alpha \tan \beta_c \quad (6)$$

According to this scheme breakdown probably occurs when the cavity length is nearly equal to the chord (since angular momentum change is rapidly decreased there), and the cavitation number for breakdown under this condition should be less than that given by equation 6.

There is the effect of blade thickness yet to consider. Let s be the spacing of adjacent blades in the cascade, and h the thickness of the blade projected onto a plane parallel to the cascade motion. The equation of continuity is,

$$V_1 s \sin \beta_1 = V_2 (s-h) \sin \beta_c \quad (7)$$

If only thickness is considered as contributing to the motion, then the velocity ratio V_1/V_2 can again be related to a possible cavitation number for breakdown as before with the result that,

$$K = 2 \left[\left(1 + \frac{h}{s} \right) \frac{\phi}{\beta_c} - 1 \right] \quad (8)$$

Equations 4, 6, and 8 are plotted in Fig. 9. In this curve, the value of the blade angle used was the blade angle at the root mean square impeller radius, and the values of flow coefficient and cavitation number are based on tip quantities. Some experimental breakdown data are also shown on Fig. 9, and it is seen that some of them lie within and along the possible breakdown regions. It is possible, therefore, that these simple models do have some usefulness. This point will be referred to again in the discussion.

B. Gas Effusion into a Cavity Bubble

A limitation imposed on the cavitation similarity parameters has been the assumption of chemical homogeneity of the fluid and the cavity bubble. Parkin and Kermeen (Ref. 4) have shown that with macroscopic cavitation and high liquid transport velocities past a cavity, significant changes can be caused in the cavity formation by the effusion of dissolved gases into the cavity bubble. Since cavity bubbles are stabilized on the impeller of a pump operating in a cavitating flow field, an investigation of the effect of air effusion on the cavity pressure was made to observe its effect on the cavitation parameter, K .

Assuming that a cavity bubble of fixed dimensions has stabilized itself on an impeller blade and that dissolved gases are present in the working fluid, equilibrium conditions are assumed to exist at the bubble, i. e., the rate of infusion of water vapor and gases into the bubble equals the rate of effusion of vapor and gases from the bubble. Entrainment of the gases is neglected; however, its effect will be to reduce the results that will be presented later.

Upon assumption of equilibrium conditions, it is possible to compute the cavity pressure of a cavitating flow field as a function of the gas concentration and temperature. Considering the cavity pressure to be summation of the partial pressures of the cavity components, the following equation can be written:

$$p_c = p_{N_2} + p_{O_2} + p_v \quad (9)$$

Using data from Ref. 10, the concentrations of N_2 and O_2 for a saturated solution in water at 760 mm mercury pressure and at $20^\circ C$, were computed and found to be 10.2×10^{-6} moles per mole of water for N_2 and 5.30×10^{-6} moles per mole of water for O_2 giving a total concentration of 15.5 moles per million moles of water.

Cavity pressures were calculated for various concentrations of air in solution using the additional assumptions that the vapor pressure of water is temperature dependent only; the concentration ratios of N_2 and O_2 in solution are temperature dependent only; and that Henry's Law applies throughout the range of gas pressures, temperatures, and concentrations of interest. Fig. 10 shows the variation of the cavity pressure as a function of gas saturation of the fluid.

In the previous discussions it has been assumed that the vapor is in equilibrium with the liquid at the same temperature. This assumption is probably never exactly realizable in a real cavity bubble since vapor is entrained at the rear of the cavity. Evaporation of the vapor as well as effusion of gas takes place into the cavity, and it may well be that the dynamics of the evaporation and entrainment process is such that the resulting pressure is less than the equilibrium pressure.

V. RESULTS AND DISCUSSION

A. Non-cavitating Performance

The non-cavitating performance map (Fig. 11) for the two impellers used in this study shows characteristics similar to those produced by inducers in commercial use (Ref. 11). Peak efficiency was obtained at a flow rate coefficient $\phi = 0.105$ for impeller one and $\phi = 0.112$ for impeller two. As anticipated, the greater tip clearance of impeller two produced a marked decrease in efficiency and head output in comparison with impeller one.

A theoretical head flow curve was computed and plotted using the simple Eulerian theory based on the mean impeller. The significant factors that cause the variation between the theoretical and experimental values of head coefficient are the non-uniform radial distribution of total head, the three-dimensional flow field, and the assumption of a perfect fluid.

Radial surveys of the downstream total head distribution were taken at flow rate coefficients of $\phi = 0.10$ and 0.14 . These data are shown in Fig. 12 where it is seen that the total head increases markedly from hub to tip. Such a distribution of total head is typical of non free-vortex blading, i. e., the downstream whirl distribution is not that of a free vortex. This result is a consequence of the helical blading used in the test impellers and the establishment of a downstream non-constant axial velocity distribution. Although a radial distribution of total head does not necessarily lead to inefficient units, it must be accounted for in designing subsequent rotor or stator stages.

At the lower flow rates, the reduced axial velocity of the flow causes the angle of attack of the tip section to rise above the stall angle. The stall on the blade generates strong radial flows towards the stalled region. These flows result in distortion of the upstream flow field by the introduction of a pre-whirl component and cause the drop in the total head at the outer radius of the passage shown in Fig. 12. The pre-whirl is thought to result from back flow from the impeller tip in the upstream direction. Additional weight for this supposition is seen in the cavitation photographs to be discussed later.

The inducer casing and impeller shaft were tufted and photographs taken at various flow rate coefficients to observe this effect. Examination of the photographs (Fig. 20) indicates the pre-whirl in the upstream flow field disappears before the flow rate coefficient reaches the peak efficiency point of the impeller. Of academic interest is the evidence of the extreme flow distortion and possible back flow caused by blade stall in both the upstream and downstream flows at the very low flow rate coefficients.

B. Cavitating Studies.

1. Performance

The cavitating performance is presented by plots (Figs. 13 through 16) of head coefficient, torque coefficient and efficiency versus cavitation number with the flow rate coefficient and impeller speed held constant. Examination of the curves reveal a continuous deterioration of head as the cavitation extent increases

for all flow rate coefficients and rotative speeds. Torque coefficients normally rise slightly as cavitation develops followed by a drop as cavitation progresses. Efficiencies generally deteriorate as the cavitation increases, however, the deterioration is not continuous but rather occurs as a rapid drop as cavitation begins to affect the flow, followed by a range of nearly constant or slightly increasing efficiency as the cavitation extent increases. Similar effects have been observed (Ref. 6), and the slight rise in efficiency is believed caused by the decrease of fluid friction as the fluid is separated from the blading. This compensating effect on efficiency is overcome as the cavitation extent further increases, and steady deterioration commences.

The conventional cavitation parameter used in hydraulic machinery literature is the suction specific speed (Appendix I). The suction specific speed developed by the experimental inducer ranged from 13,500 to 15,400 for an impeller speed of 6,000 rpm and flow rate coefficients of $\phi = 0.08$ and 0.14 , respectively. At impeller speeds of 9,000 rpm, the suction specific speeds obtained were 24,400 to 18,800 for the flow rate coefficients 0.08 and 0.14 , respectively. The decrease in the suction specific speed with an increase in flow rate at 9,000 rpm is a result of the breakdown of the service plumbing, which did not permit the application of low absolute suction pressures to the system.

Wislicenus gives a maximum value of suction specific speed of 8,140 for non-cavitating flow in axial flow pumps (Ref. 3). Ross and Banerian have reported results on cavitating inducers operating at suction specific speeds of 65,000 (Ref. 11).

Comparison of results obtained during these studies shows that the head coefficient-cavitation number curves are similar to the head-suction specific speed given by Ross and Banerian for a typical inducer. The lower suction specific speeds reported here are a result of a relatively high blade angle and a high hub ratio (0.5).

2. Photographic and Visual Studies

Five general regimes of cavitation were observed during cavitation development on the experimental impellers. These were classified as inception and tip cavity cavitation, tip cavity and vortex cavitation, unsteady alternate blade cavitation, steady alternate blade cavitation, and fully developed cavitation on all blades. The various regimes are shown in Figs. 21 through 30, which are series of photographs detailing cavitation development for both impellers at the various parametric conditions.

To permit a concise presentation of the photographic data and correlate the visual observation with the photographic data, Figs. 17, 18 and 19 were prepared to map cavitation development. The boundaries shown are, of course, very approximate. Since observations were taken for incremental decreases of the suction pressure, it is possible, although unlikely, that other significant cavitation regimes exist that were not observed.

The first stage of cavitation observed was the formation of a tip cavity, and occurred for all values of flow rate coefficient and impeller speed. The actual inception point for visible cavitation exhibited strong dependence on the flow rate coefficient and tip clearance. This dependence indicated that the cavitation was initiated by the higher angle of attack occurring at the blade tip

and was suppressed by the increased tip clearance. As the angle of attack of the flow was reduced, lower values of the cavitation number were required to obtain cavitation inception.

After cavitation inception, further reduction of the cavitation number increased the size of the tip cavity until the transition to the next cavitation regime occurred. At the lower flow rates, the next regime appearing was the tip and vortex cavities. This particular regime is best demonstrated in Figs. 21 and 25. The initial appearance of the vortex cavity is parallel with the plane of rotation; however as cavitation extent is increased, the size of the vortex cavity increases, and complex interactions of the various flows cause an upstream advance and a radial displacement of the cavity towards the hub of the inducer. Figs. 17, 18 and 19 suggest that the phenomenon is closely related to the tip clearance flows and to the angle of attack of the incoming fluid. The abrupt disappearance of the vortex cavity after the flow rate coefficient passes the peak efficiency point of the impeller is indicative that the pre-whirl of the fluid combined with the radial flows caused by non free-vortex blading are initiators of the vortex. In addition, it appears that the tip clearance flows increase the vortex cavity strength (cf. Figs. 21 and 25).

The next two regimes of cavitation are believed to be essentially similar with one being the limiting case of the other. The limiting case is considered steady alternate blade cavitation. The cavities are such that very large cavities are attached to alternate blades, and the blades immediately adjacent have very

small cavities (cf. Figs. 23, 24 and 30). This regime occurred only for the higher values of flow rate coefficient investigated and through a narrow range of the cavitation number. The other regime is very similar except that the cavitation becomes unstable, and occurs at the lower flow rates. Strong cavitation is observed on alternate blades, however the large cavities do not remain on the same blade but shift from one blade to the blade immediately adjacent. Since a four-bladed impeller was used, it could not be ascertained if the shifting of the large cavity was by continuous rotation around the impeller or by means of an oscillatory motion.

No satisfactory explanation for this behavior is available; however, its similarity to the rotating stall encountered in axial flow machines would suggest a similar mechanism. Under conditions not yet known, the disturbance propagates from one passage to another. Due to the very low aspect ratio of the blades on the impellers studied, it is likely that tip clearance effects are important in this phenomenon, since the extent of the unstable region varied significantly for the two values of tip clearance used (Figs. 17 and 18).

The shifting of the cavity appeared periodic and the frequency was observed to be a function of the flow rate and the suction pressure of the fluid. Inception occurred with a frequency estimated at about 30 cycles per second and decreased to approximately two to five cycles per second as the suction pressure was reduced. The oscillations appear to cause weak dynamic effects at the higher frequencies; however, as the frequency of the phenomenon decreases, the dynamic effects become very noticeable.

At the lower frequencies, these effects caused strong vibrations throughout the entire facility, and the power requirement of the pump became very unsteady.

The final regime in cavitation development is the appearance of fully developed cavities on all blades of the impeller (Figs. 21, 22, 28 and 31). The cavity length approaches the blade chord length and the inducer becomes dynamically unstable in the generation of head, maintenance of flow rate or the absorption of torque. In this situation, impeller breakdown is either occurring or is imminent. The boundaries for this regime seem to be practically independent of the flow rate and impeller speed suggesting that it is or should be possible to define this regime of cavitation by the use of a pressure coefficient alone.

3. Tip Clearance Effects

The impellers used for the cavitation studies were nearly identical except for the differences in the tip clearance. Impeller one was manufactured with the minimum tip clearance that could be attained with normal manufacturing methods. Impeller two was manufactured with a tip clearance established at the optimum value of the tip clearance parameter suggested by Rains (Ref. 5). This parameter was defined by the ratio of the tip clearance to the maximum blade tip thickness and was shown to control the inception point of cavitation in an axial flow pump. Cavitation inception was shown to occur for a minimum value of the cavitation parameter when the value of the tip clearance parameter was 0.1.

The increase of the tip clearance to obtain the desired

value of the tip clearance parameter for impeller two produced the anticipated results on the non-cavitating performance of the impeller. Marked reductions were observed for the efficiency and head output of the impeller.

Examination of Figs. 15 and 16 showed that the performance of impeller two as cavitation became extensive was similar to that of impeller one except that the various effects observed for impeller one occurred at significantly lower values of the cavitation number than for impeller one. This is demonstrated more graphically in Figs. 17 and 18 in the shift of the boundaries of the cavitation regime. Of interest is the shift of boundaries for the cavitation regimes shown in Figs. 18 and 19, suggesting that the rotational speed of the machine must be considered in the selection of an optimum value for the tip clearance parameter, although the reason for this behavior is not known.

The shift in the boundaries of the cavitation regimes is believed to be caused by complex interactions of the tip clearance flows and the radial flows occurring at the outer edges of the impeller. In the region of tip and vortex cavity formation, it is believed that the tip clearance flows reinforce the radial flows producing the vortex cavity (cf. Figs. 21 and 25). The kinematics of the flow field motion are so complex at this stage of cavitation development and flow rate coefficient that no complete explanation can be given at this time. However, it seems probable that the advance of the vortex cavity upstream and its radial displacement is due to the pre-whirl observed in the tuft patterns (Fig. 20), and illustrates the development of back flows. Certainly further experimental investigation of the phenomenon is needed.

4. Impeller Breakdown

Impeller breakdown data could not be obtained conclusively for the majority of the experimental runs made because of the service pump system limitations or instability of the entire facility at the breakdown condition. A few points of genuine breakdown were obtained and are shown in Fig. 9.

The region of possible impeller breakdown obtained by the use of the simple theoretical models proposed for the description of breakdown lies outside of the majority of the experimental values obtained. Two suggestions are offered to account for this discrepancy; first, all the photographs, Figs. 21 through 31, indicate that three-dimensional flows are present and may cause local reductions of the cavitation number within the impeller, and second, the cavitation numbers computed may be in considerable error from the use of the water vapor pressure as the cavity pressure. Some aspects of the effect of the presence of dissolved gases on cavity pressure were given in Section IV and the magnitudes and direction of the error possible in the computation of the cavitation number are such that the true value of the local cavitation number may be considerably less than the value computed.

Figure 31 gives excellent corroboration to the model of impeller breakdown occurring when the cavity fills the fluid passages within the impeller. It can be seen that the cavities extend to nearly the full length of the impeller blade chord and also extend radially from the tip to the hub of the impeller. Thus, even though the actual flow pattern in an impeller at breakdown is highly confused, a general resemblance to the simple models proposed is

retained within the actual flow pattern. It is possible that further refinements of these simple models presented may result in better agreement. The breakdown criterion given by equation 4 is seen to be much too optimistic whereas that of equation 6 is sometimes high and sometimes low.

Ultimately, of course, the three-dimensional effects must be considered in any more complete theory. This problem, however, is beyond the scope of the present work.

5. Cavitation Scaling.

Cavitation modeling using the Prandtl cavitation number for a pump operating at different speeds is shown by Figs. 15 and 16. to be essentially correct with a maximum variation of the hydraulic output parameters being less than five percent.

The effect of dissolved gases was not considered in the computation of the values of the cavitation number. Since the air content of the water used for the experimental studies was maintained nearly constant, i. e., the air content varied from 2.5 to 3.5 ppm, the cavitation numbers computed for comparison of the various parametric conditions probably are correct relative to each other. However, the computed values of the cavitation number could show considerable variation from the true cavitation number if it had been possible to measure the cavity pressure.

Using the techniques discussed in Section IV, cavitation numbers were computed using the equilibrium cavity pressure for a few representative experimental points. For an impeller rpm of 6,000 and a flow rate coefficient $\phi = 0.10$, the value of the cavitation number using an assumed air content of 2.5 ppm at 20° C.

was 0.0387. The same point, using the vapor pressure of the fluid as the cavity pressure, was computed to have a cavitation number of 0.115. Thus a computation of cavitation number based on an equilibrium cavity pressure was 66 percent lower than the number based on fluid vapor pressure alone. Another value computed showed the cavitation number based on an equilibrium pressure to be -0.015, the value based on the fluid vapor pressure to be 0.059, or a variation of over 108 percent. It is realized that equilibrium conditions are never attained in a cavity but the variations shown above indicate that, when operating at very low suction pressures and with dissolved gases present in the working fluid, some consideration should be given to a better estimation of the cavity pressure if cavitation scaling is to be correctly accomplished. This is particularly true if blended fluids having a significant rise of temperature on the distillation curves are being pumped.

VI. CONCLUSIONS

The simple helix impellers used for the cavitation studies exhibited non-cavitating and cavitating characteristics similar to conventional inducers in present use, and hence, results obtained from this study are considered applicable to inducers of conventional design. Cavitation development was separated into five distinct regimes occurring between cavitation inception and impeller breakdown. These regimes are:

1. tip cavity formation,
2. tip and vortex cavity formation,
3. unsteady alternate blade cavitation,
4. steady alternate blade cavitation,
5. full cavitation development on all blades.

The noise and vibration characteristics of cavitating pumps were found to occur principally in only one regime of cavitation, i. e. unsteady alternate blade cavitation, and the location of this particular regime on a cavitation development map for this impeller could be changed significantly by a change of flow rate through the pump or a change of the tip clearance of the impeller.

Cavitation scaling using the Prandtl cavitation number is realized in a highly cavitating flow field. Suggestions are presented to modify the accepted definition of the cavitation number by attempting to account for gaseous effusion into the cavities in a flow at very low suction pressures.

A simple model based on a cavitating cascade is used to define impeller breakdown and some correlation is obtained between the experimental data and model values. Photographs

indicate that the same general cavity formation is present in an impeller at breakdown as described by the model. Experimental evidence is shown that breakdown should be modeled primarily by the use of a pressure coefficient such as the cavitation number.

REFERENCES

1. Jet Propulsion, Air Technical Service Command (1946).
2. Sutton, J. P., Rocket Propulsion Elements, John Wiley and Sons, Inc. (1949).
3. Wislicenus, G. F., Fluid Mechanics of Turbomachinery, McGraw Hill Book Company (1947).
4. Parkin, B. R. and Kermeen, R. W., "Incipient Cavitation and Boundary Layer Interaction on a Streamlined Body", Report E-35.2, December 1953, Hydrodynamics Laboratory, California Institute of Technology.
5. Rains, Dean A., "Incipient Cavitation in Axial Flow Pumps, Part I: "Tip Clearance Flows and Incipient Cavitation", Report E-56.1, March 1954, Hydrodynamics Laboratory, California Institute of Technology.
6. Guinard P., Fuller T., Acosta, A. J., "An Experimental Study of Axial Flow Pump Cavitation", Report E-19.3, August 1954, Hydrodynamics Laboratory, California Institute of Technology.
7. Kermeen, R. W., "Some Observations of Cavitation on Hemispherical Head Models." Report E-35.1, June 1952, Hydrodynamics Laboratory, California Institute of Technology.
8. Betz, A., and Petersohn, E., "Anwendung der Theorie der freien Strahlen", Ingenieur Archiv, Band II (1931).
9. Peters, J. P. and Van Slyke, D. D., "Quantitative Clinical Chemistry, Vol. II, Williams and Wilkins Co. (1932).

10. Handbook of Chemistry and Physics, Thirtieth Edition,
Chemical Rubber Publishing Co. (1947).
11. Ross, C. C. and Banerian, G., "Some Aspects of High
Suction Speed Inducers", Paper 55-A-124 read at the
ASME Diamond Jubilee Meeting, Chicago, Ill.,
Nov. 1955.

APPENDIX I

- A Area of flow passage
- c Axial component of the flow velocity
- d Lineal distance
- F Force
- g Acceleration of gravity--32.2 ft./sec.²
- h Cascade blade thickness projected onto the plane of cascade motion
- H Hydraulic head, feet of water
- k Any arbitrary constant
- K Prandtl cavitation number = $\frac{p_1 - p_v}{\frac{1}{2} \rho V_1^2}$
- N Revolutions per minute
- p Pressure
- P Power
- Q Volume flow of fluid, ft.³/sec.
- r Radial distance from centerline of impeller shaft
- s Spacing between adjacent blades of the cascade
- S_v Suction specific speed = $\frac{N (446 Q)^{1/2}}{NPSH^{3/4}}$
- T Torque
- u Lineal impeller velocity
- v Flow velocity relative to the impeller
- W Specific weight of fluid
- α Flow angle of attack = $\beta_c - \beta_1$
- β Flow angle measured from the plane of rotation of the impeller
- η Efficiency of the pump = $\frac{\psi \phi}{\tau}$
- σ Thoma cavitation parameter = $\frac{NPSH}{H}$

τ Torque coefficient = $\frac{T}{\rho A u_2^2 r_2}$

ϕ Flow rate coefficient = $\frac{Q}{A u_2}$

Ψ Total discharge head coefficient = $\frac{H g}{u_2^2}$

c. p. s. Cycles per second

NPSH Net positive suction head = $H_1 - H_v$

Subscripts:

0 Impeller mid-section

1 Impeller hub, also conditions far upstream

2 Impeller tip, also conditions within the impeller

c Blade chord

v Fluid vapor

APPENDIX II

DETERMINATION OF NON-DIMENSIONLESS PARAMETERS

The requirements for similarity of turbomachinery as given by Wislicenus (Ref. 3) are broken down into two criteria: (1) the fundamental considerations of geometric similarity of the machines and the kinematic similarity of the flow field through the machines and (2), the similarity considerations created by the physical properties of the fluid passing through the machine, i. e. viscosity, vapor pressure, compressibility, surface tension, etc.

The implications of kinematic similarity of the flow field are, in addition to the geometric similarity of the machines, that the velocity distributions of the fluid throughout the entire flow field be similar. Thus, the force distributions as applied by the machine to the fluids must be similar. The fundamental considerations can be expressed as:

$$\frac{d_a}{d_b} = k \quad (10)$$

$$\frac{\left[\frac{V}{U} \right]_a}{\left[\frac{V}{U} \right]_b} = k \quad (11)$$

From the above it is seen that the fluid velocities must maintain a constant ratio with the impeller tip velocities for similarity. Converting the fluid velocity to the more familiar appropriate quantity of fluid flow, equation 11 reduces to:

$$\frac{\left[\frac{Q/d^2}{Nd} \right]_a}{\left[\frac{Q/d^2}{Nd} \right]_b} = k \quad (12)$$

or as a non-dimensional parameter:

$$\frac{Q}{Nd^3} = k \quad (13)$$

Further manipulation will give the conventional hydraulic non-dimensional flow parameter ϕ :

$$\frac{Q}{Nd^3} = \frac{Q}{Nr_2A} = \frac{Q}{AU_2} = \phi \quad (14)$$

Similarly, the forces exerted by the impeller on the fluid can be converted to the conventional non-dimensional head parameter, ψ . The force imparted on the fluid can be given as:

$$F = \rho Q \Delta V = \rho A V \Delta V \quad (15)$$

Since ΔV must be proportional to the fluid velocity V passing through a cross-sectional area, the equation can be given as

$$p = \frac{F}{A} = k \rho V^2 \quad (16)$$

Converting to the normal hydraulic head,

$$H = \frac{p}{W} = \frac{k V^2}{g} \quad (17)$$

or

$$\frac{gH}{U_2^2} = \psi \quad (18)$$

It is realized that other forces such as viscosity are

eliminated in the derivation of the constants, but these relations have shown excellent empirical agreement (Ref. 3) with the analysis just presented provided that the dimensions of the turbomachine are large, the compressibility of the fluid is small, the viscosity is small, and cavitation is not present.

The hydraulic power produced by the pump is equal to the flow rate Q displaced against a hydraulic pressure WH per unit time or:

$$P = WHQ \quad (19)$$

or by substitution:

$$P = \psi \phi \left[\frac{WA u_2^2}{g} \right] \quad (20)$$

If the input power is given as a product of torque and rpm,

$$P = NT = \frac{u_2 T}{2\pi r_2} \quad (21)$$

and then the torque is converted to a non-dimensional coefficient by the following relation:

$$\tau = \frac{T g}{WA u_2^2 r_2} \quad (22)$$

then the efficiency of the pump can be given directly as:

$$\eta = \frac{\psi \phi}{\tau} \quad (23)$$

The cavitation similarity parameter used was the cavitation number as initially defined by Prandtl, i. e.

$$K = \frac{P_1 - P_v}{\frac{1}{2} \rho V_2^2} \quad (24)$$

The relative tip velocity can be expressed in terms of the various flow by the following relation:

$$V_2^2 = C^2 + U_2^2 \quad (25)$$

but:

$$C = \frac{Q}{A} = \frac{\phi}{U_2} \quad (26)$$

$$V_2^2 = U_2^2 (1 + \phi^2) \quad (27)$$

For convenience in computation of the cavitation number the use of another common hydraulic parameter, the net positive suction head, is employed where:

$$NPSH = H_1 - H_v \quad (28)$$

then by appropriate manipulation:

$$K = \frac{P_1 - P_v}{W} \frac{2g}{V_2^2} \quad (29)$$

$$K = \left(\text{NPSH} - \frac{c^2}{2g} \right) \frac{2g}{V_2^2} \quad (30)$$

$$K = \frac{2\text{NPSH} k_2 - \phi^2}{\phi^2 + 1} \quad (31)$$

where k_2 is defined as the ratio $\frac{e_3}{U_2^2}$.

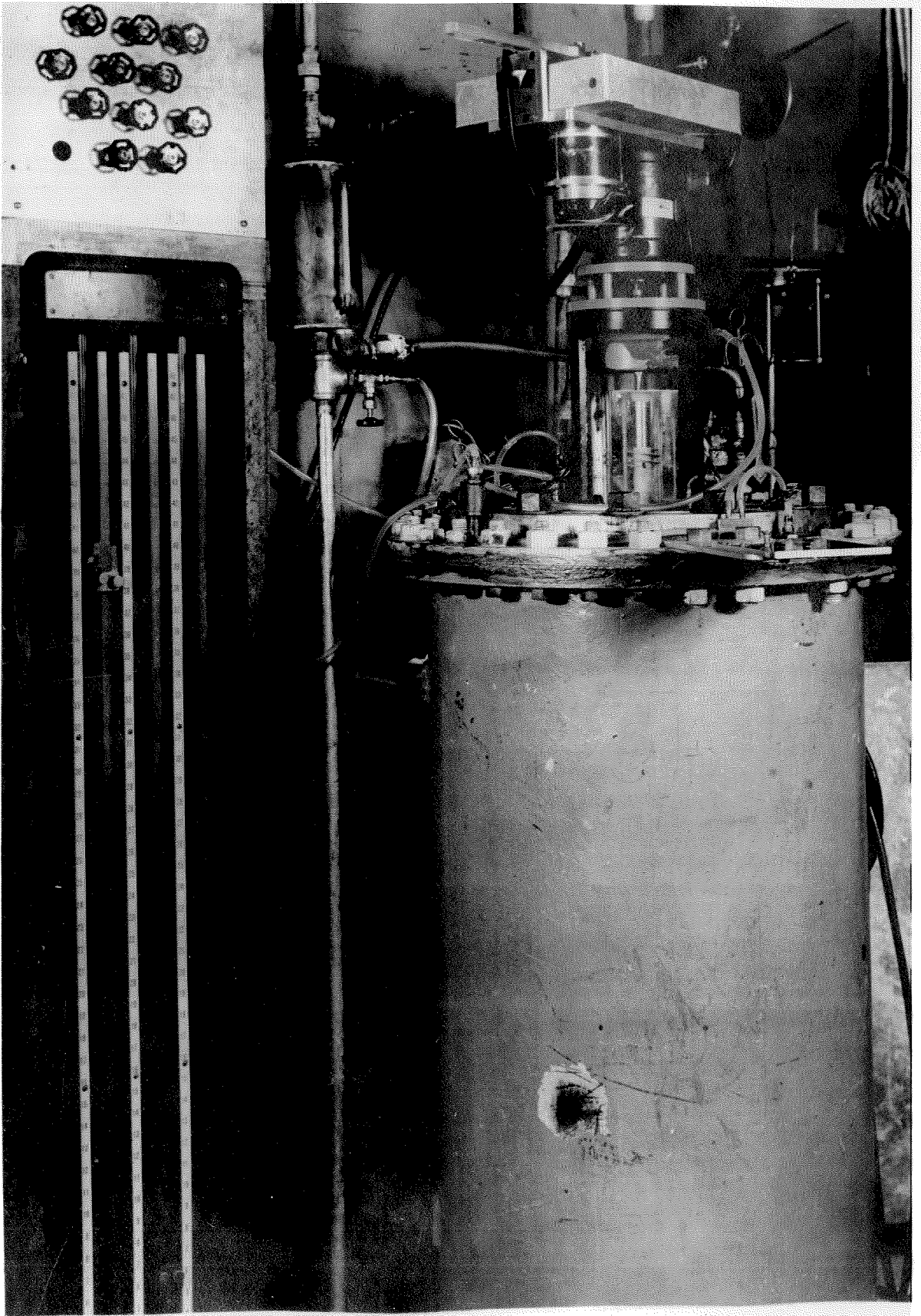


FIG. 1 AXIAL INDUCER FACILITY

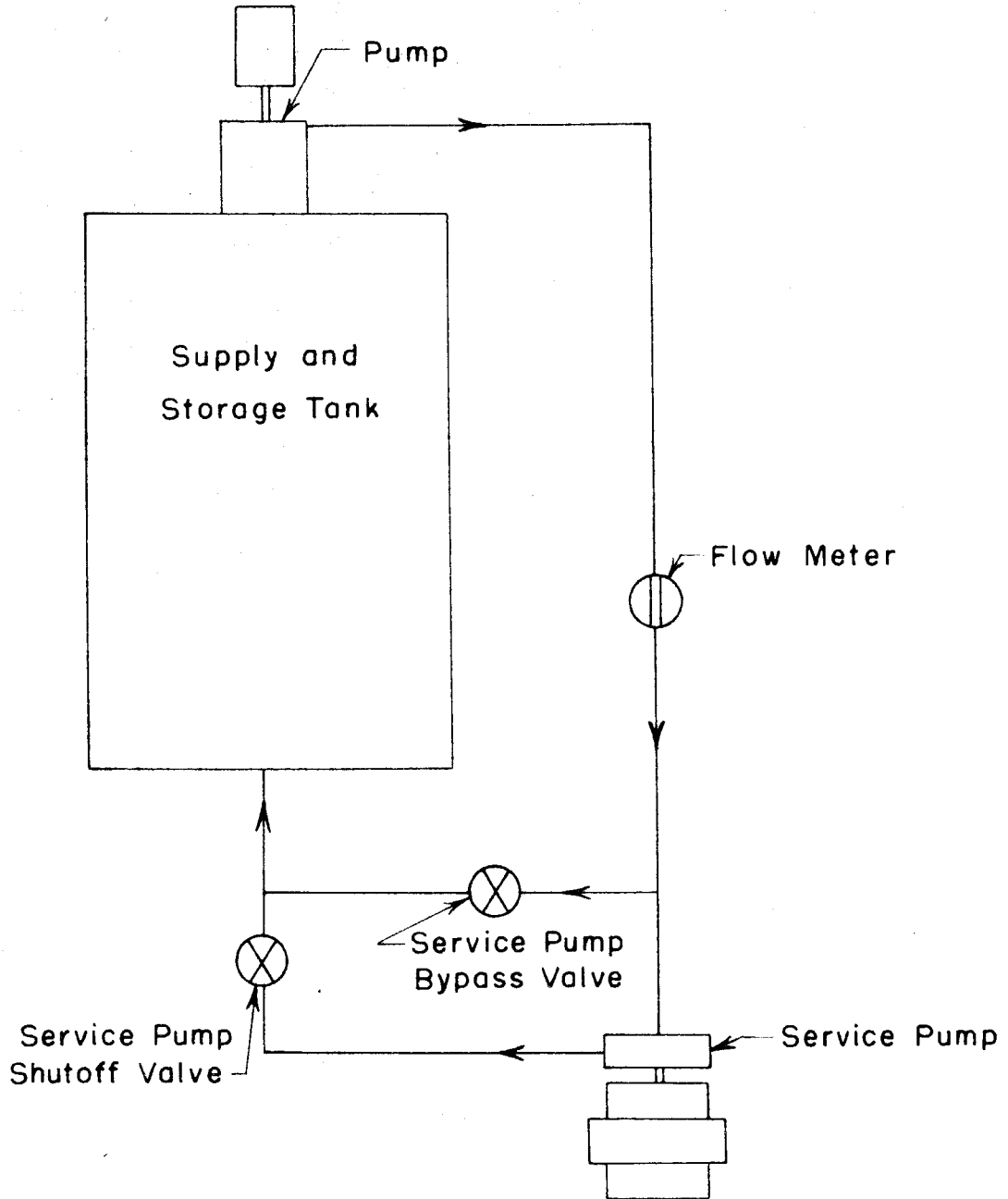


FIG. 2 - FLOW DIAGRAM - AXIAL INDUCER FACILITY

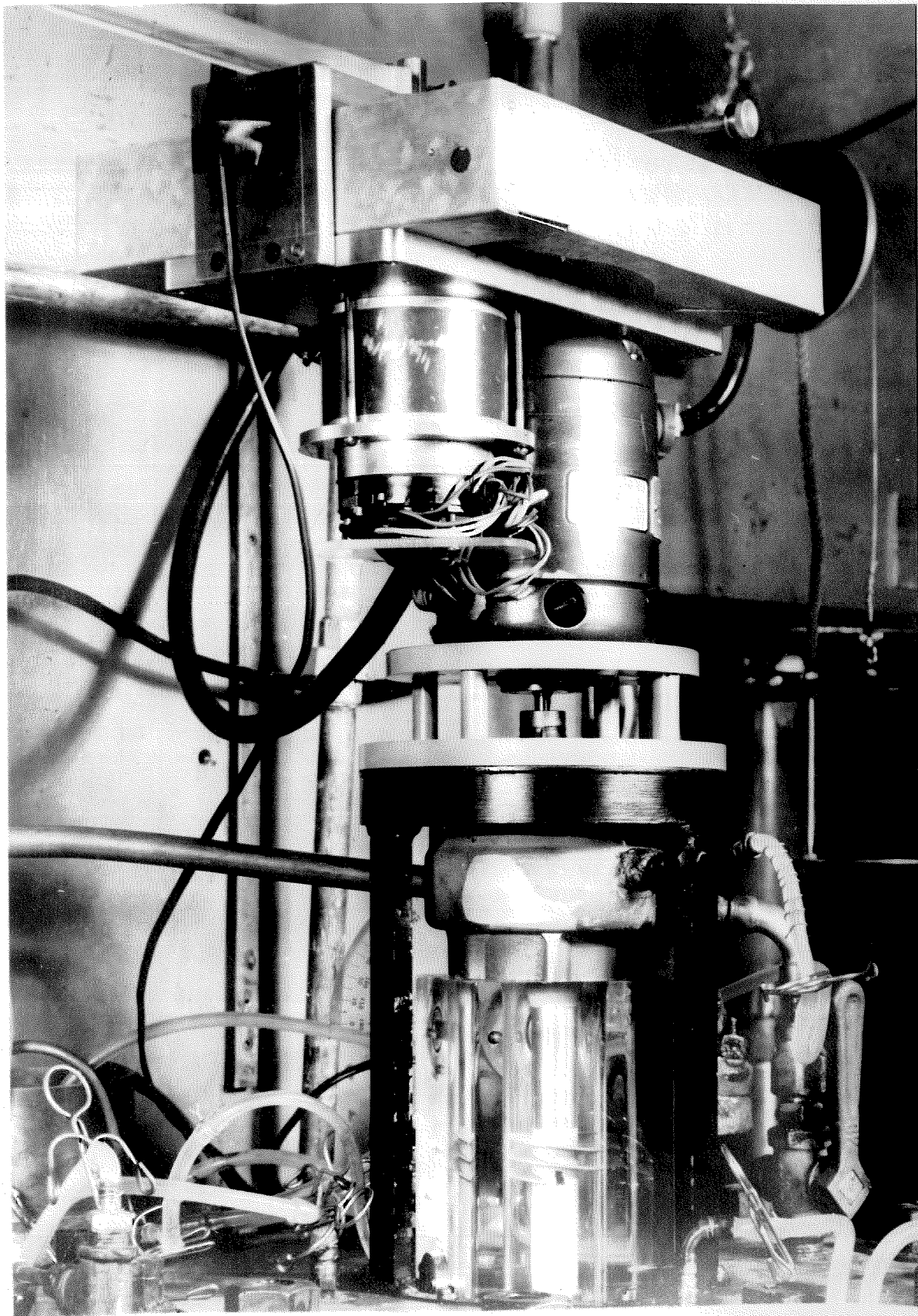
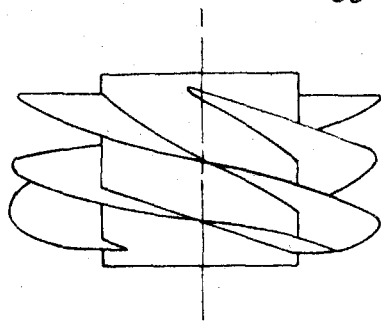
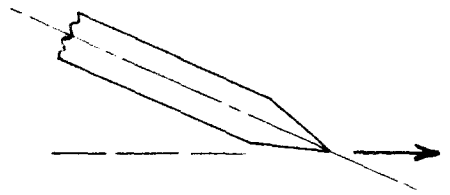


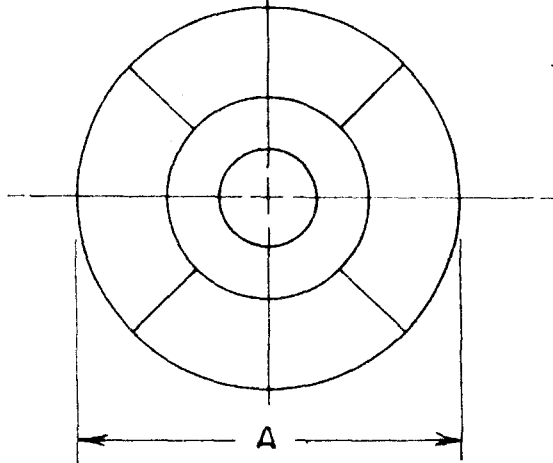
FIG. 3 MOUNTING DETAILS, AXIAL D-CER



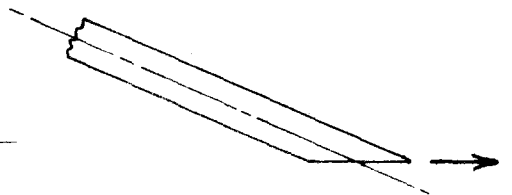
Impeller Side View



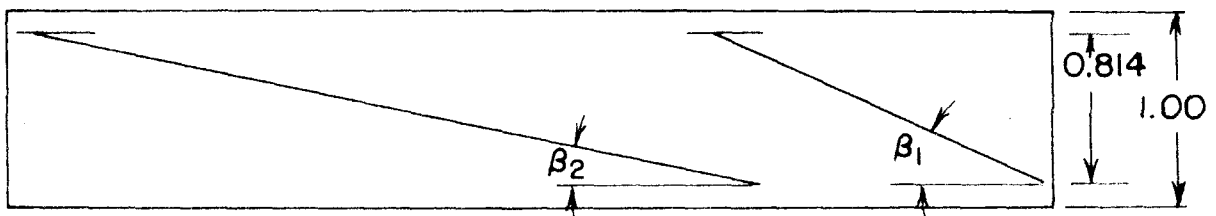
Leading Edge - Impeller No.1
(Not To Scale)



Impeller - Bottom View



Leading Edge - Impeller No.2
(Not To Scale)



Hub And Tip Blade Pitch Lines

Dimension	Impeller No.1	Impeller No. 2
A	1.996 "	1.991 "
β_1 (Hub)	23.10 °	23.10 °
β_2 (Tip)	12.05 °	12.05 °
Blade Thickness		
Hub	0.035 "	0.035 "
Mid Radius	0.041 "	0.041 "
Tip	0.047 "	0.047 "

FIG. 4 - IMPELLER DETAILS

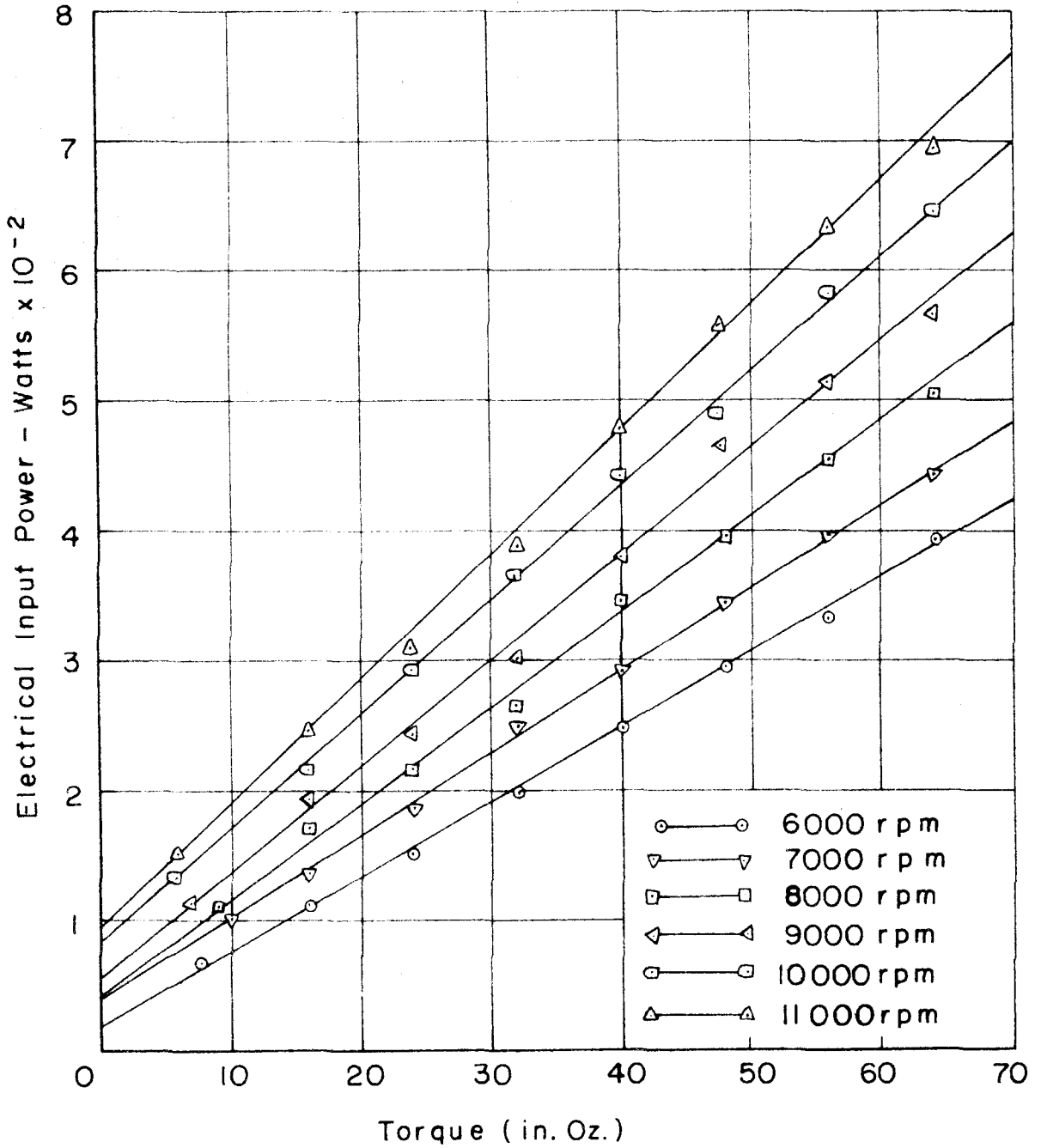


FIG. 5 - CALIBRATION OF DRIVE MOTOR

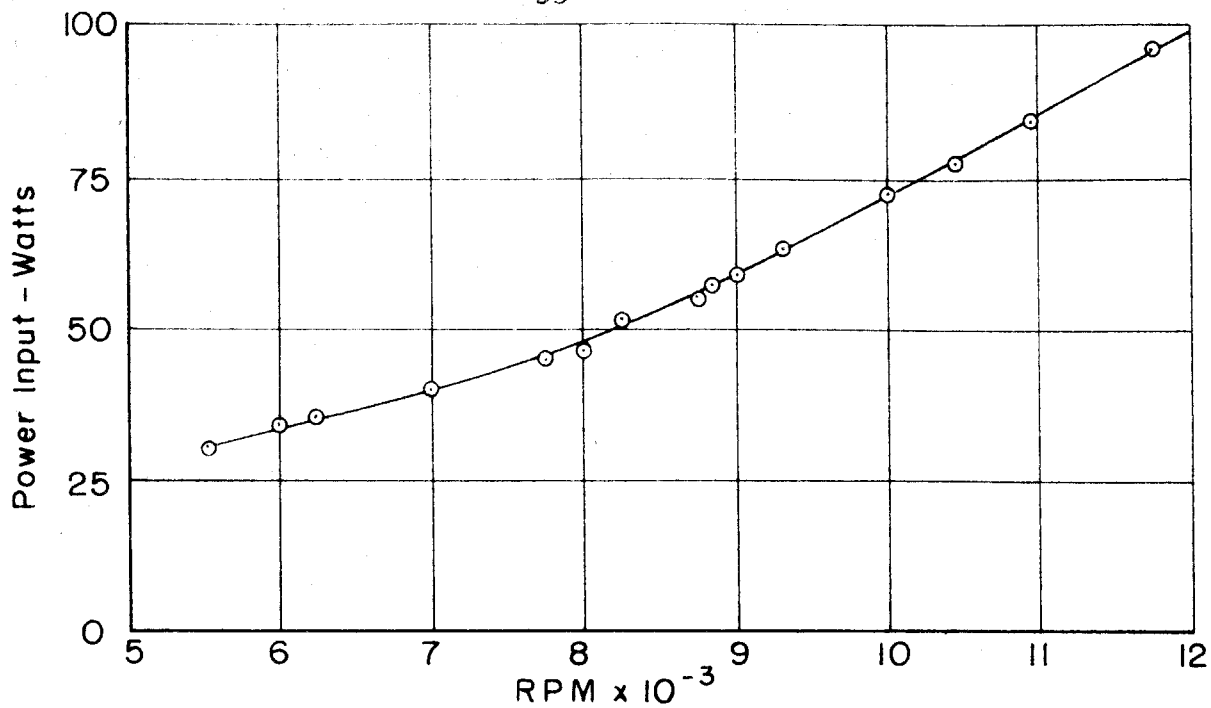


FIG. 6 - NO LOAD MOTOR CHARACTERISTIC

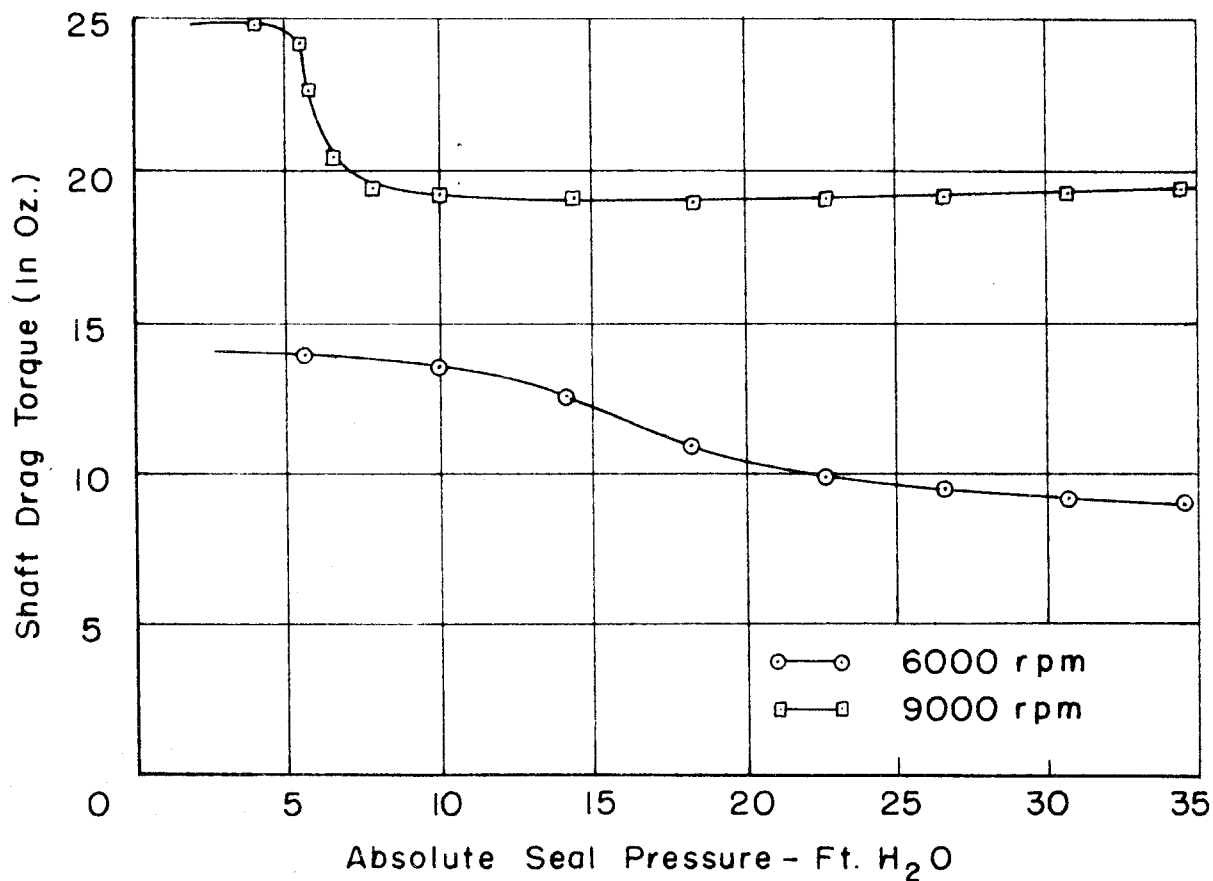


FIG. 7 - VARIATION OF SHAFT DRAG TORQUE WITH SEAL PRESSURE

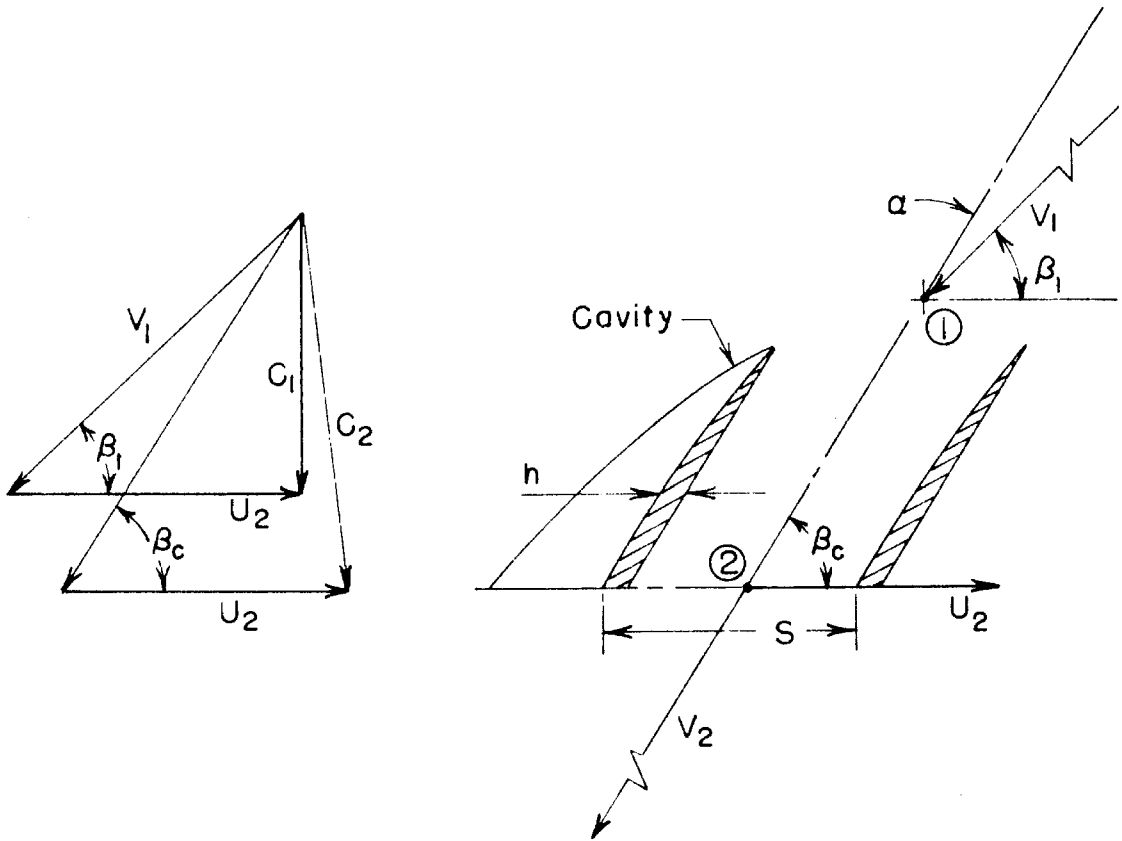


FIG. 8 - VELOCITY DIAGRAM AND DEFINITIVE SKETCH FOR A CASCADE OR AXIAL FLOW PUMP

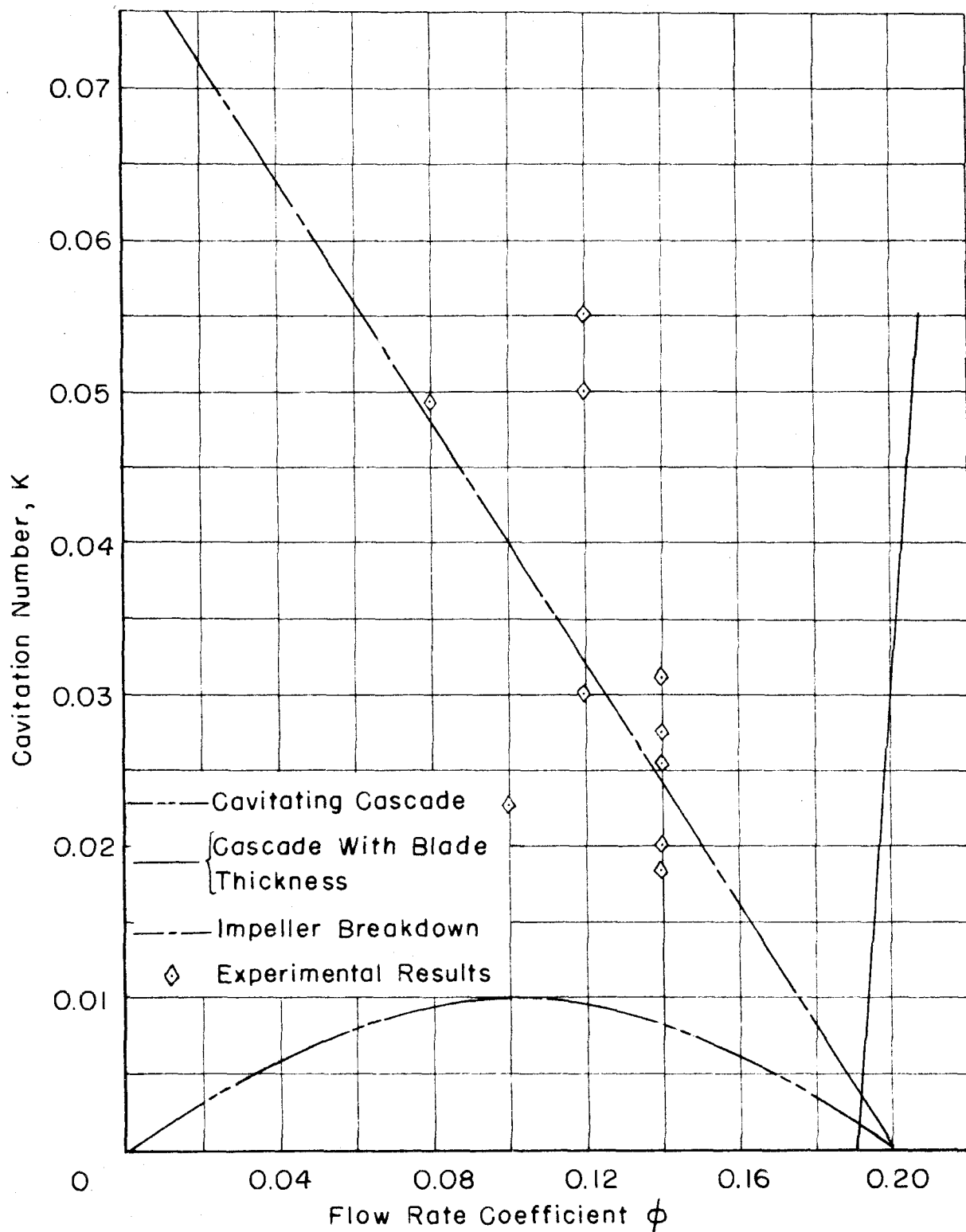


FIG. 9 - BREAKDOWN CAVITATION FOR THE AXIAL INDUCER

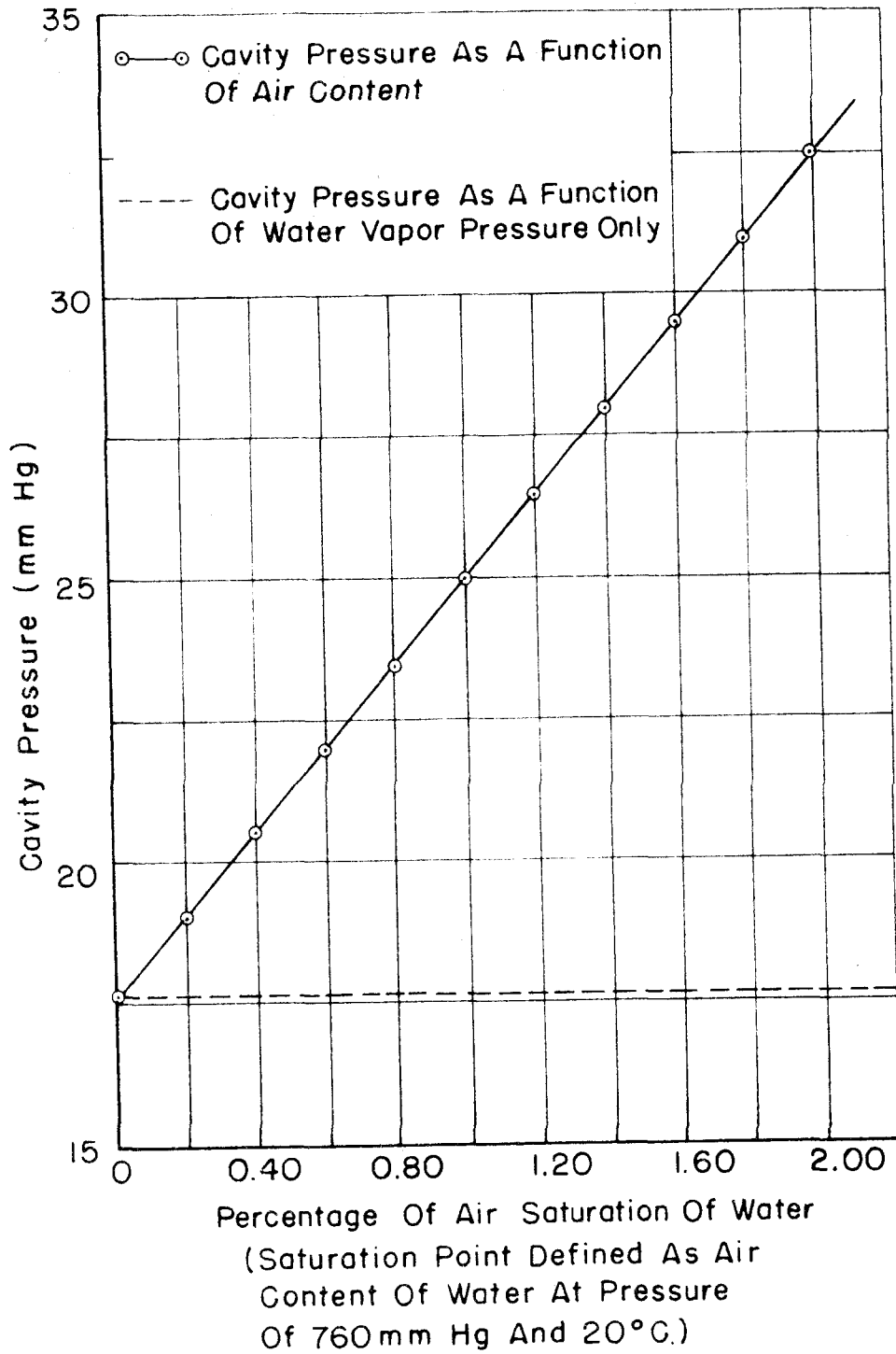
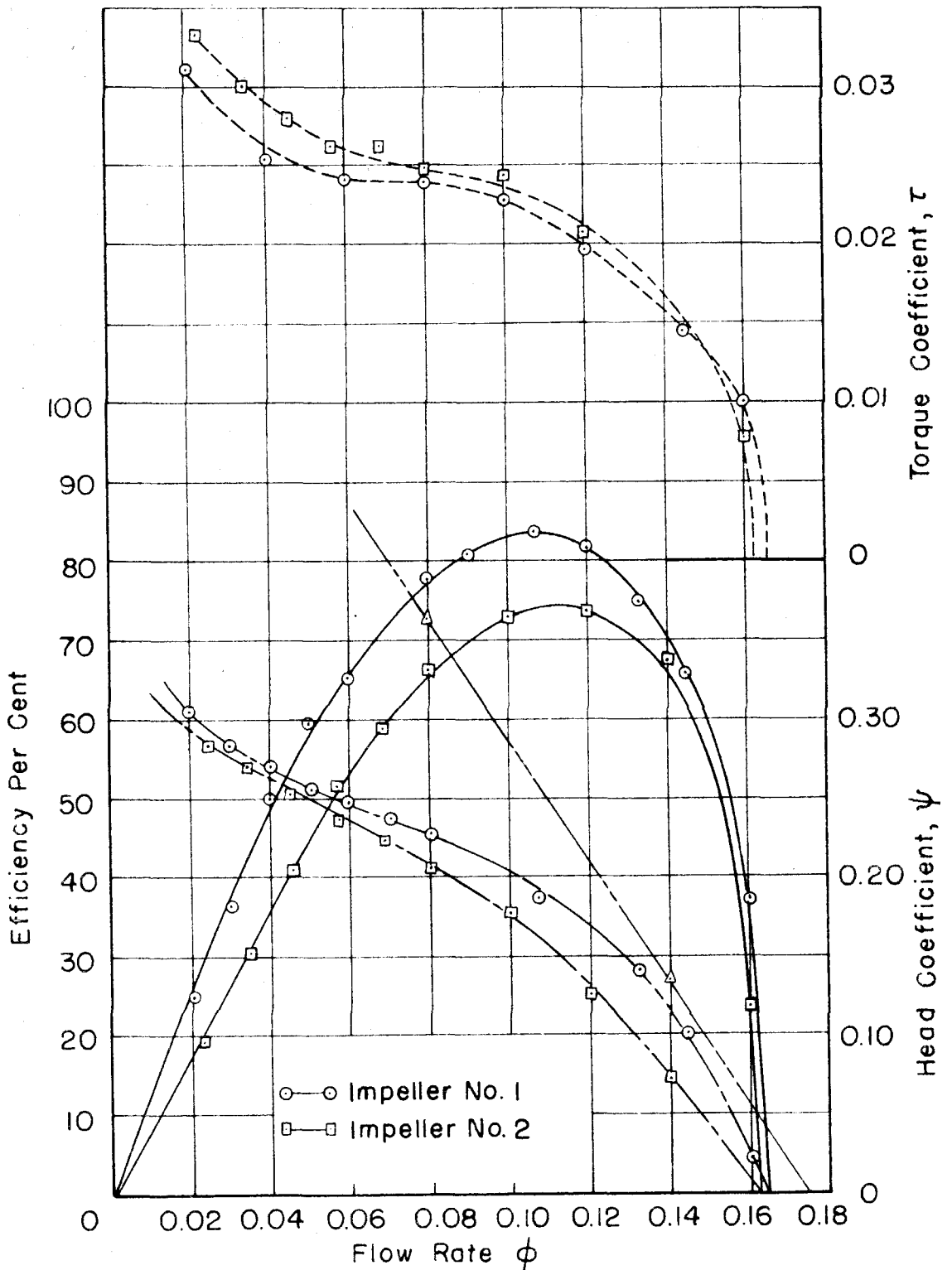


FIG.10- CHANGE OF CAVITY PRESSURE BY EFFUSION OF DISSOLVED AIR



— Efficiency ——— Torque Coefficient τ
 - - - Head Coefficient ψ { Theoretical Head (Simple Euler Theory)

FIG. II - NON CAVITATING CHARACTERISTICS - AXIAL INDUCERS

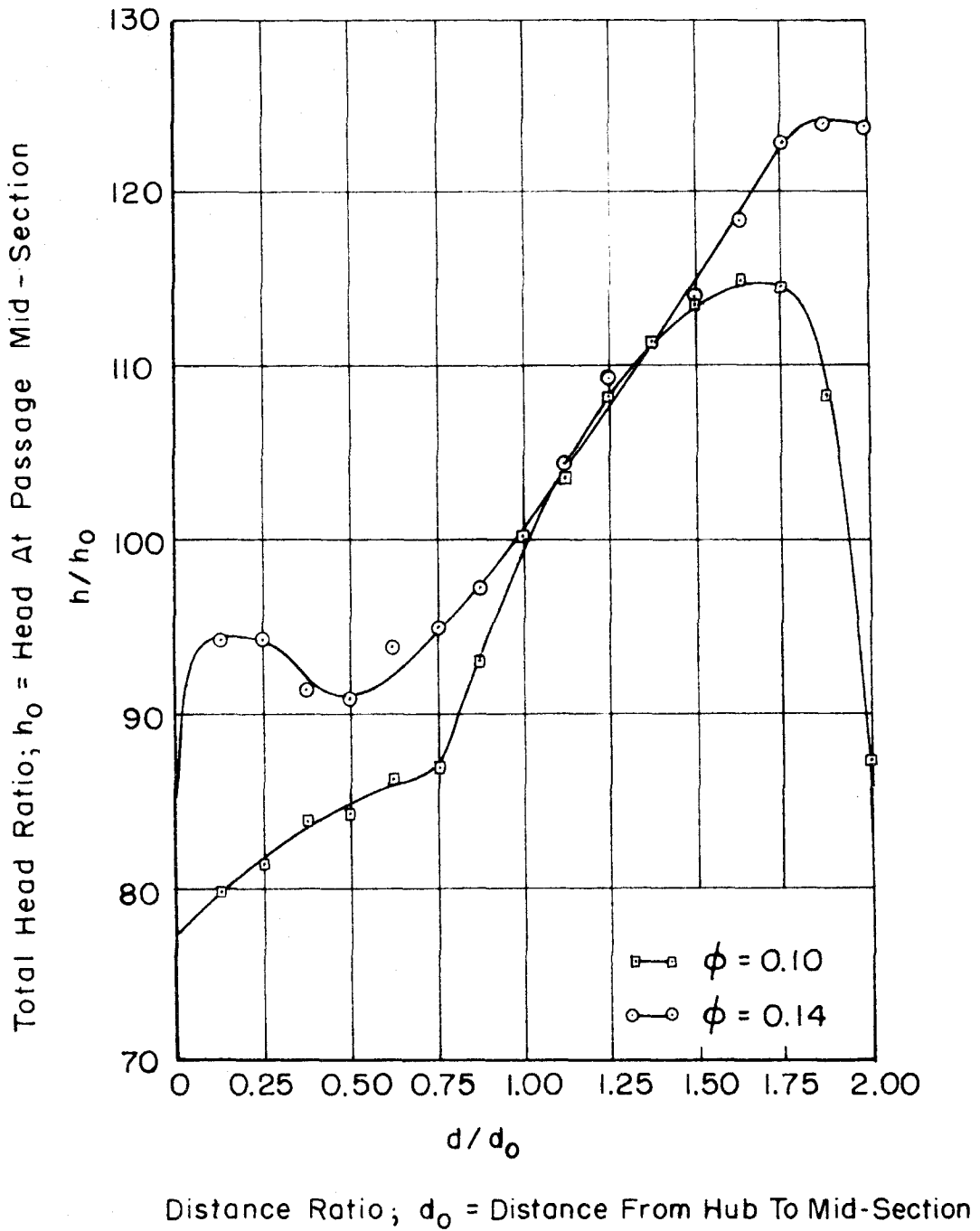


FIG. 12 - RADIAL DISTRIBUTION OF TOTAL HEAD DOWNSTREAM OF THE IMPELLER

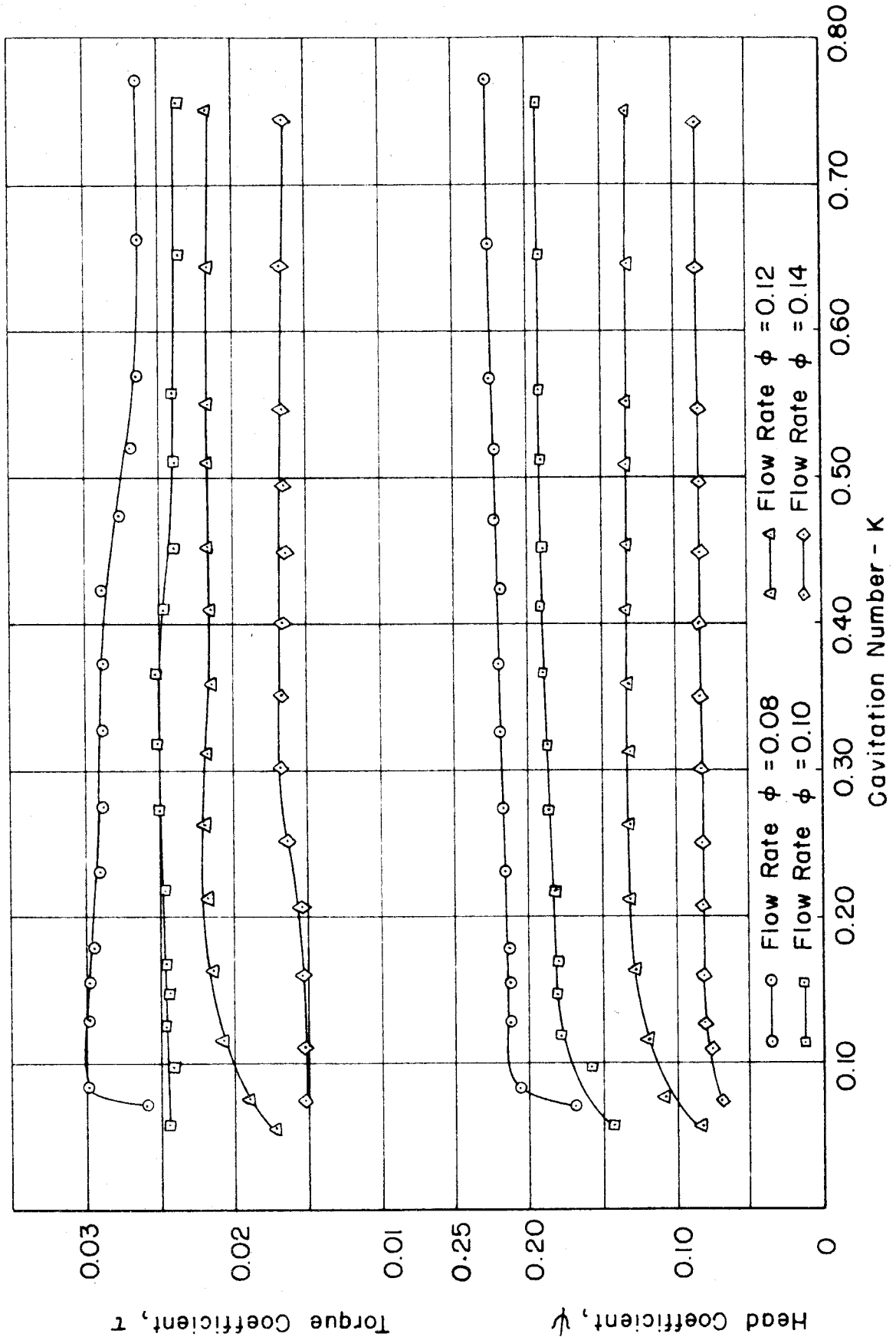


FIG.13-CAVITATING CHARACTERISTICS-IMPELLER NO.1

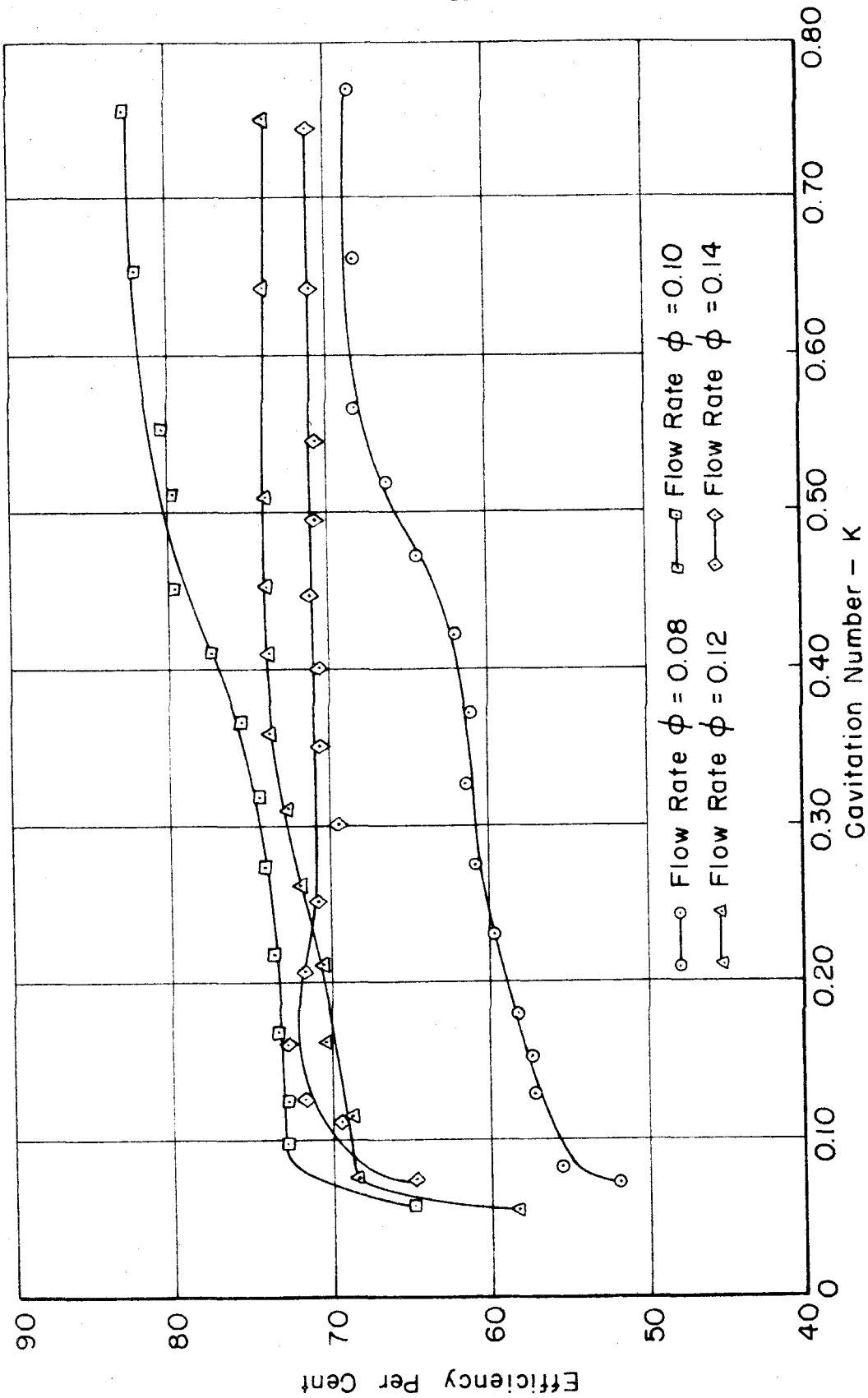


FIG. 14 - CAVITATING CHARACTERISTICS - IMPELLER NO. 1

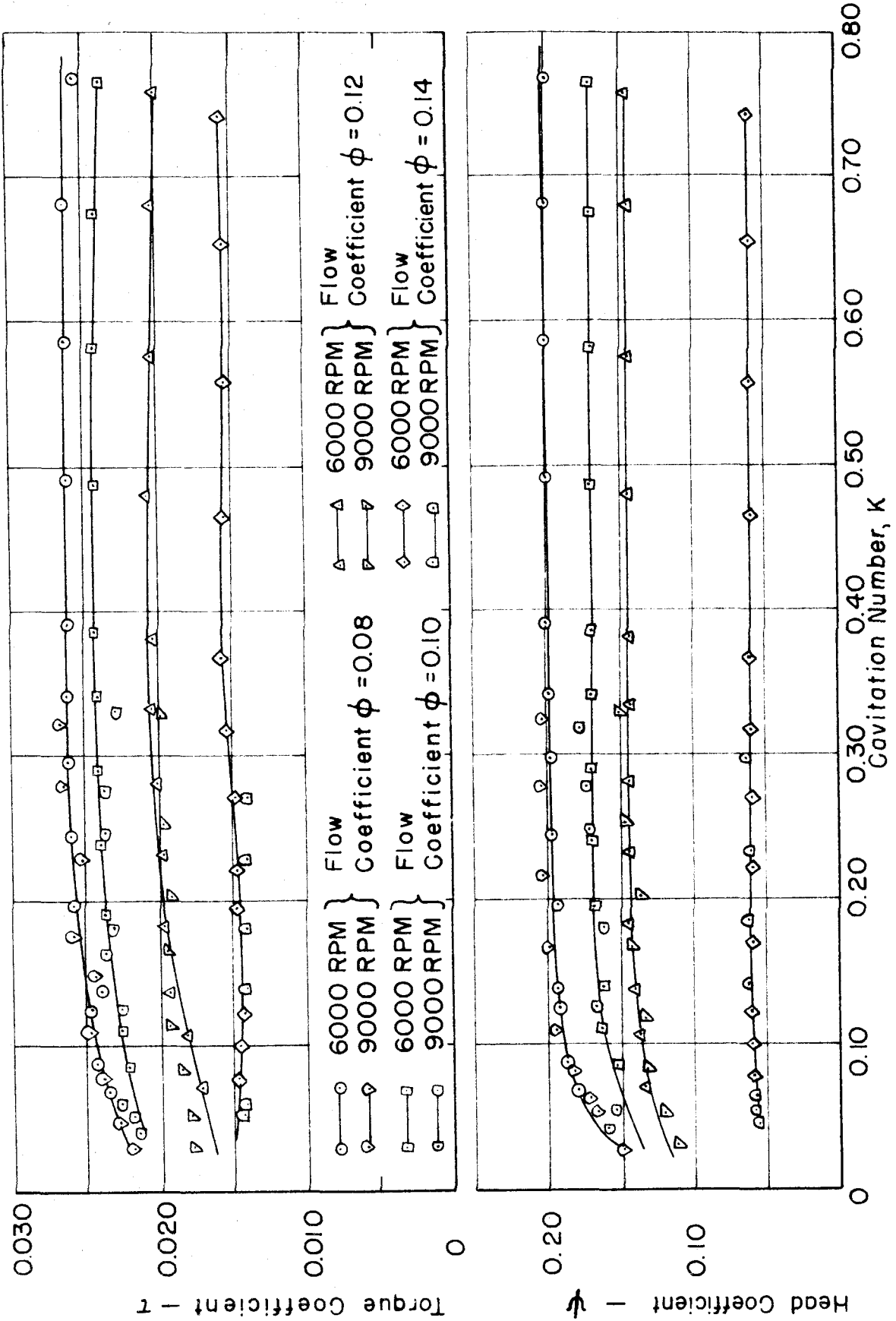


FIG. 15 - CAVITATING CHARACTERISTICS - IMPELLER NO. 2

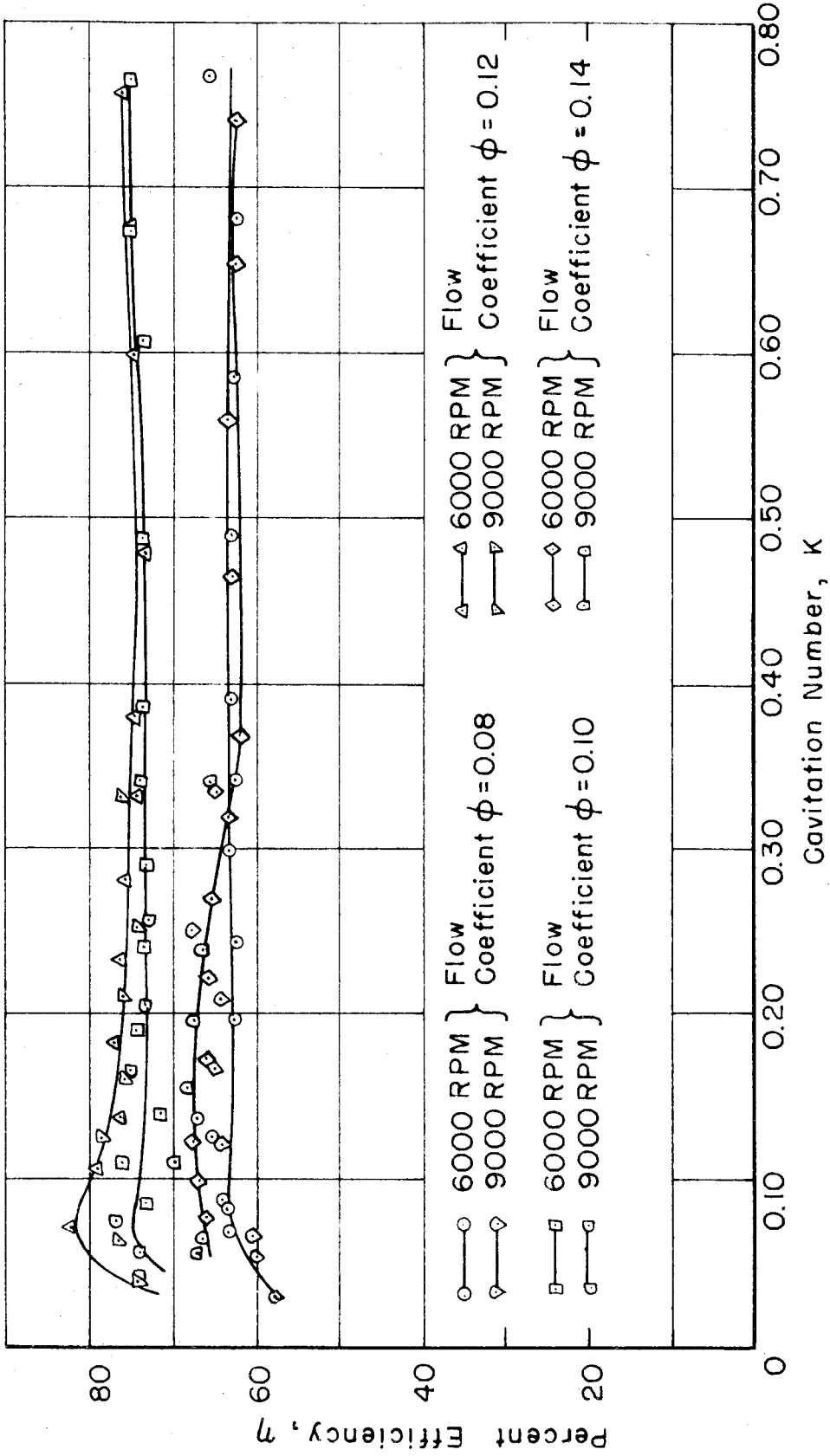
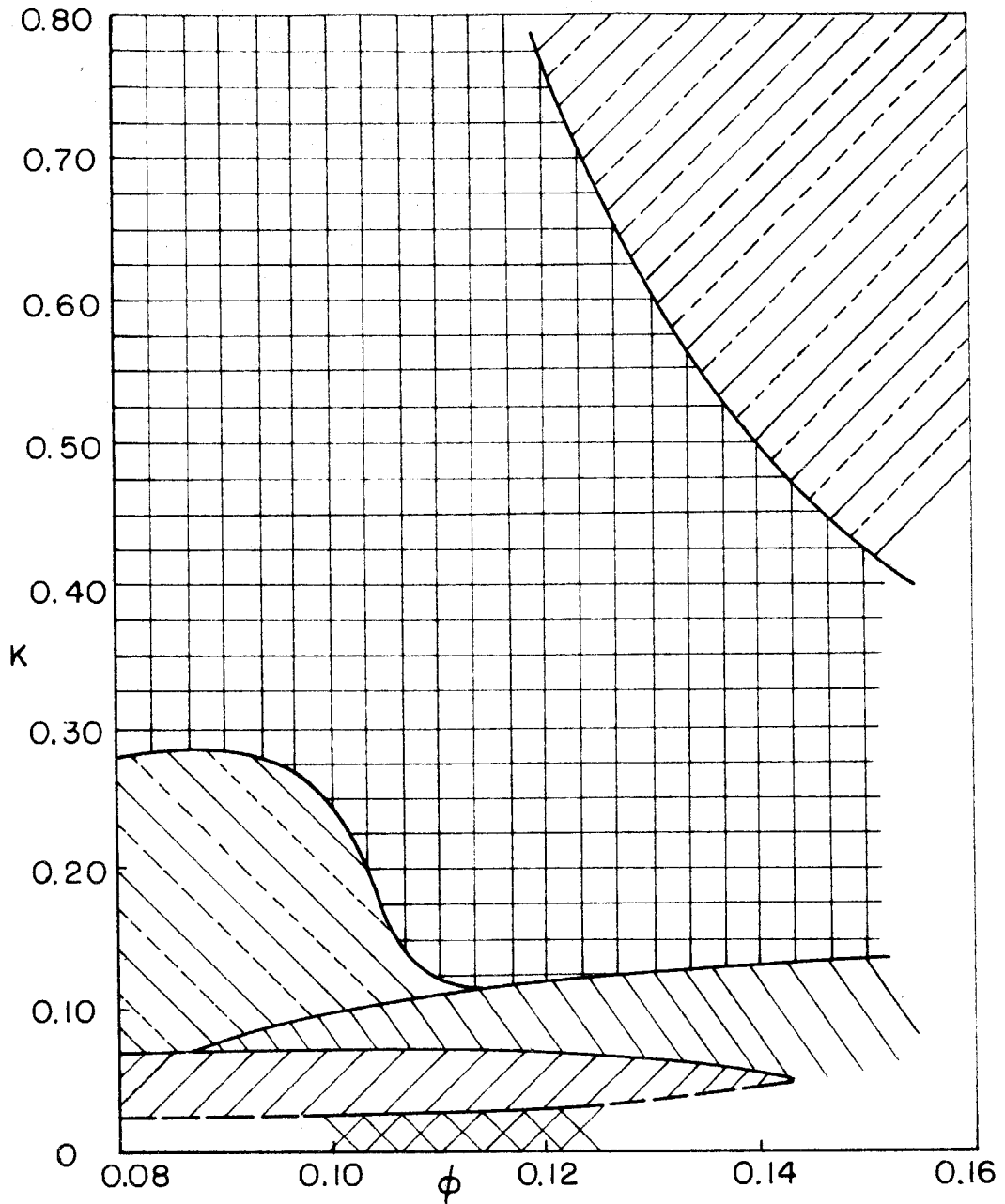


FIG. 16 - CAVITATING CHARACTERISTICS - IMPELLER NO. 2



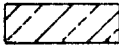
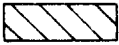


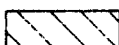

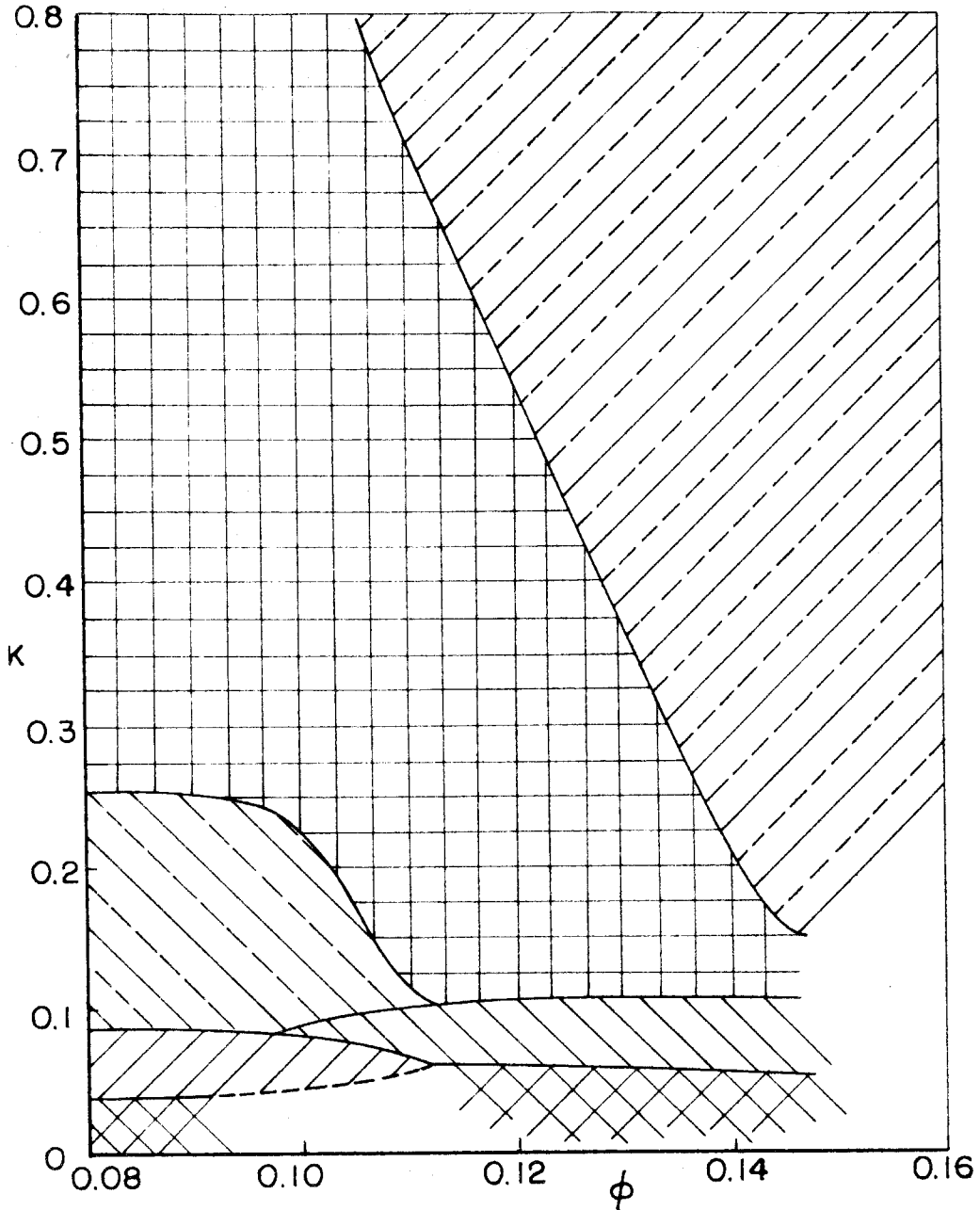
- | | |
|--|--|
|  No Visible Cavitation |  Alternate Blade Cavitation |
|  Cavitation At Blade Tips |  Unsteady Alternate Blade Cavitation |
|  Tip Cavitation And Vortex Generation |  Fully Developed Cavitation All Blades |

FIG. 17 - CAVITATION DEVELOPMENT AT 6000 RPM
IMPELLER NO. 1



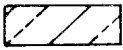


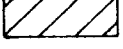
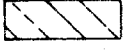
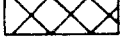
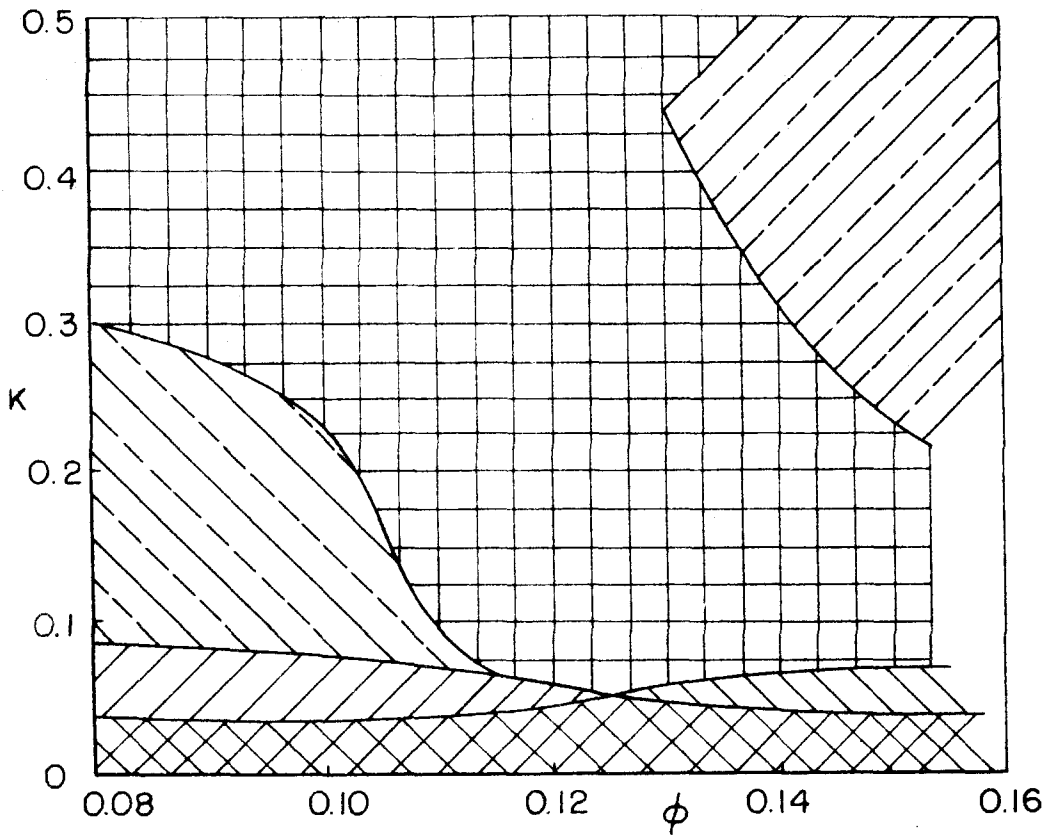
- | | |
|--|---|
|  No Visible Cavitation |  Alternate Blade Cavitation |
|  Tip Cavitation At Blade Tips |  Unsteady Alternate Blade Cavitation |
|  Tip Cavitation And Vortex Generation |  Fully Developed Cavitation All Blades |

FIG. 18 - CAVITATION DEVELOPMENT AT 6000 RPM
IMPELLER NO. 2



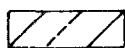
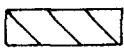


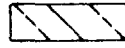
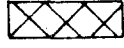
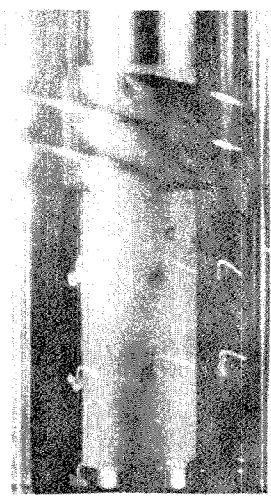
- | | |
|--|---|
|  No Cavitation Visible |  Alternate Blade Cavitation |
|  Cavitation At Blade Tips |  Unsteady Alternate Blade Cavitation |
|  Tip Cavitation And Vortex Generation |  Fully Developed Cavitation All Blades |

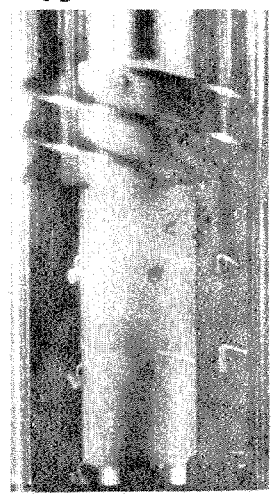
FIG. 19 - CAVITATION DEVELOPMENT AT 9000 RPM
IMPELLER NO. 2



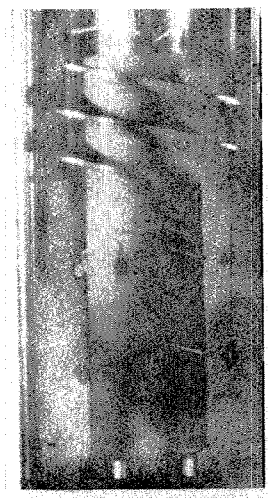
$\phi = .033$



$\phi = .033$



$\phi = .047$



$\phi = .047$



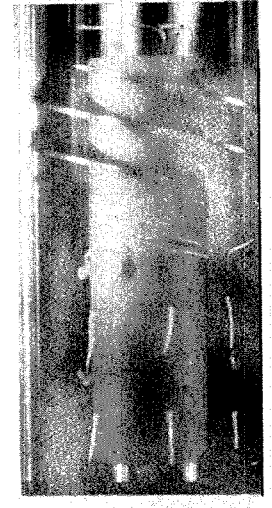
$\phi = 0.060$



$\phi = 0.060$



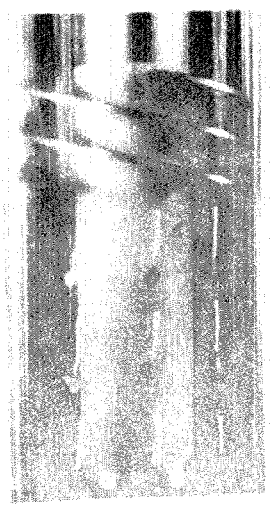
$\phi = 0.080$



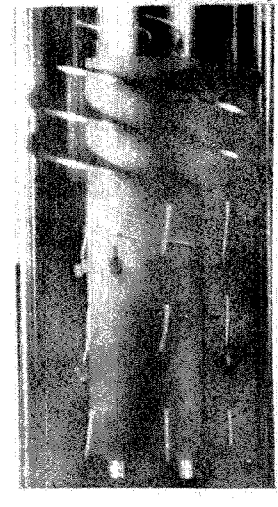
$\phi = 0.080$



$\phi = 0.100$

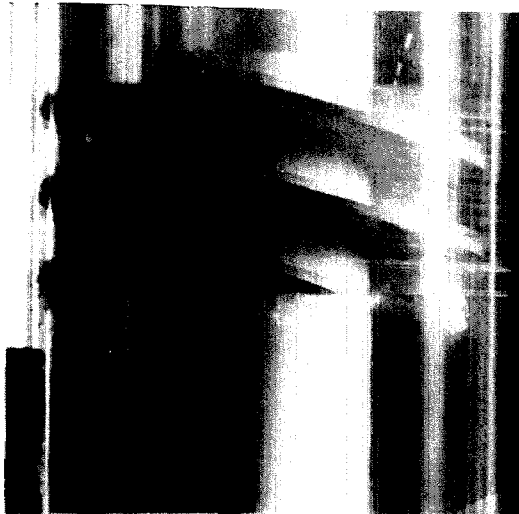


$\phi = 0.100$



$\phi = 0.120$

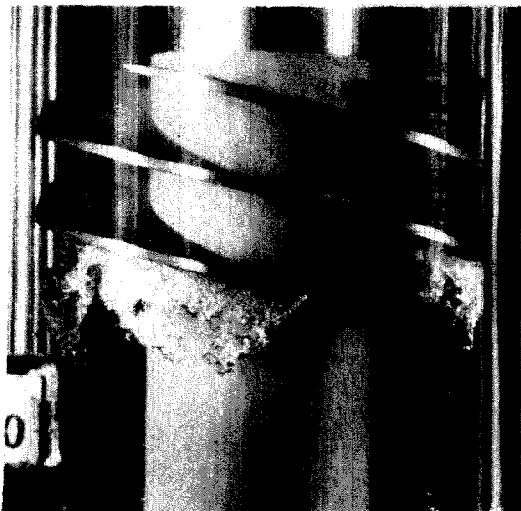
FIG. 20 NON-CAVITATING FLOW THROUGH IMPPELLER ONE



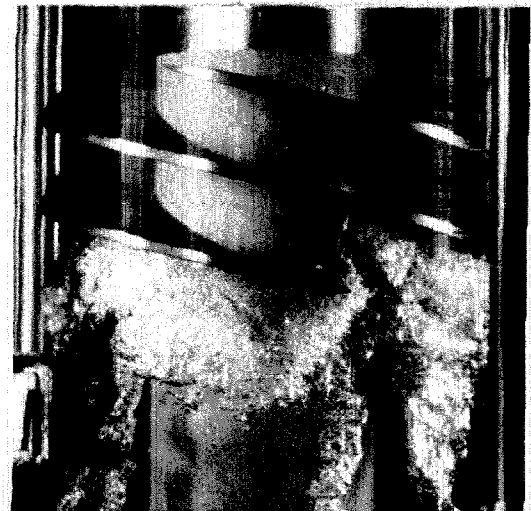
K = 0.372



K = 0.274



K = 0.154

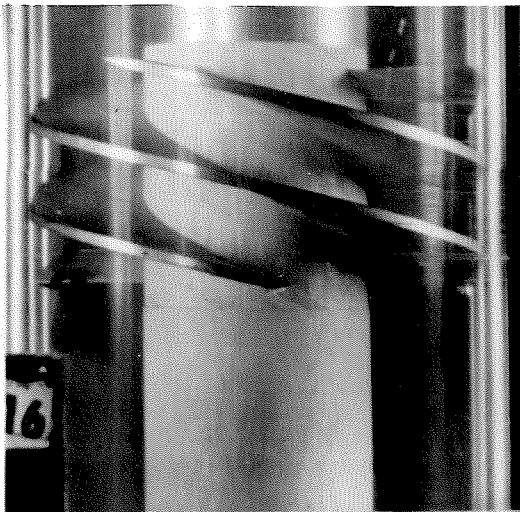


K = 0.084

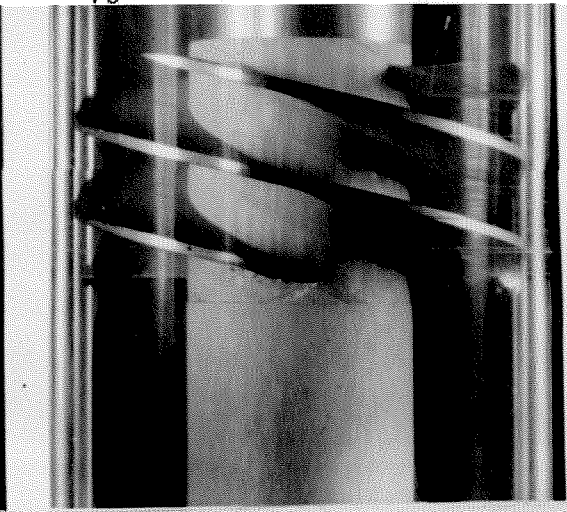


K = 0.071

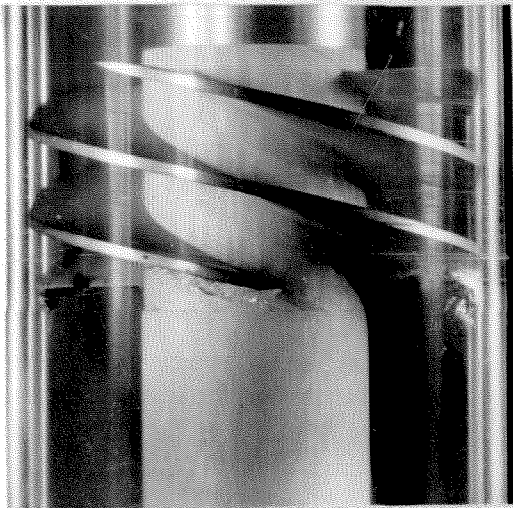
FIG. 21 CAVITATION DEVELOPMENT, IMPELLER ONE
 $\Phi = 0.08$, RPM 6000



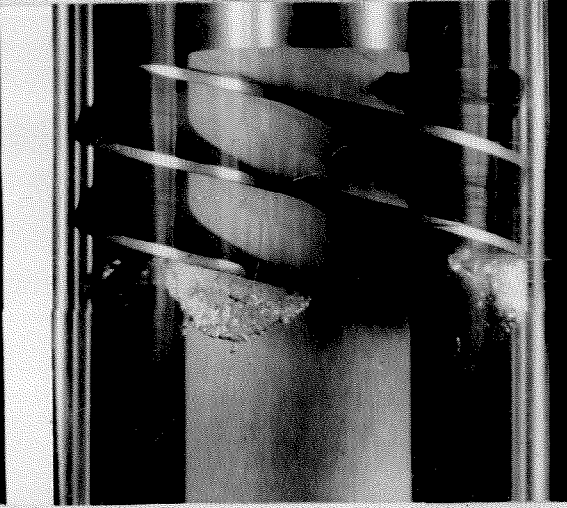
$K = 0.757$



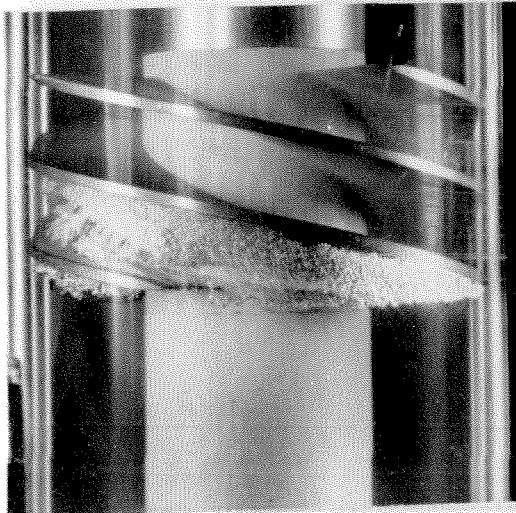
$K = 0.452$



$K = 0.318$



$K = 0.218$

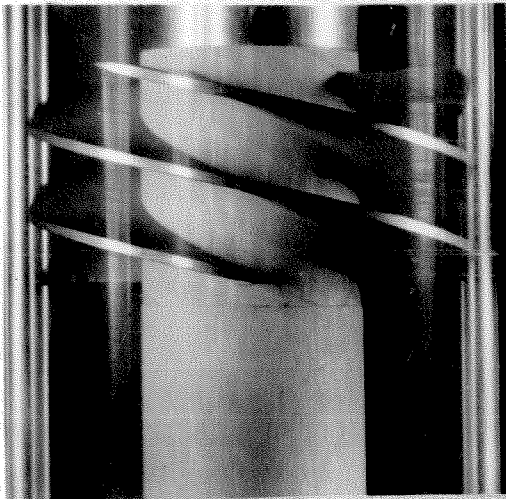


$K = 0.098$

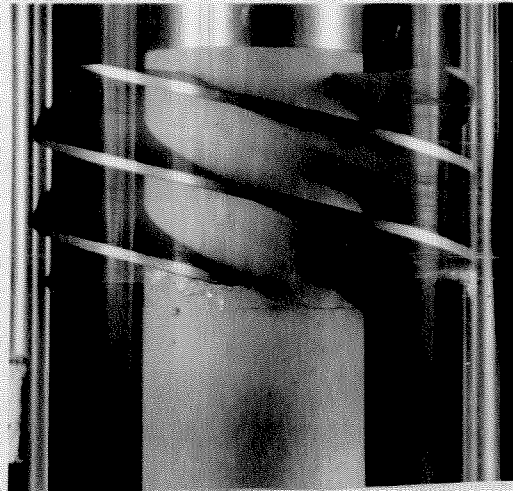


$K = 0.056$

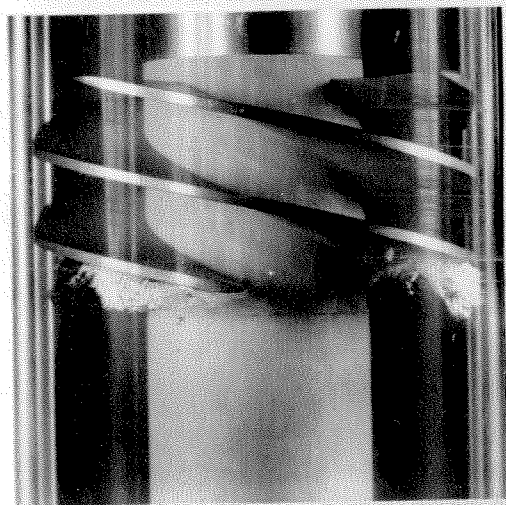
FIG. 22 CAVITATION DEVELOPMENT, IMPELLER ONE
 $\Phi = 0.10$, RPM 6000



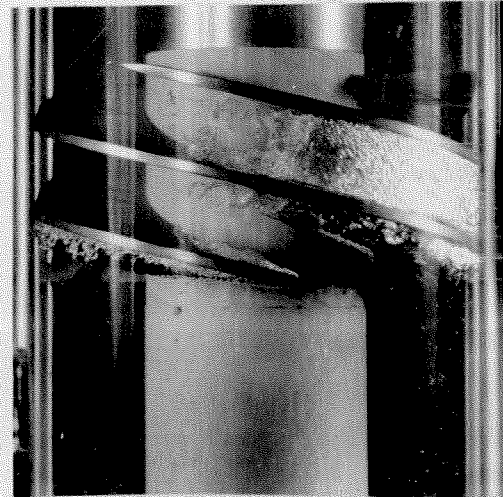
$K = 0.751$



$K = 0.358$

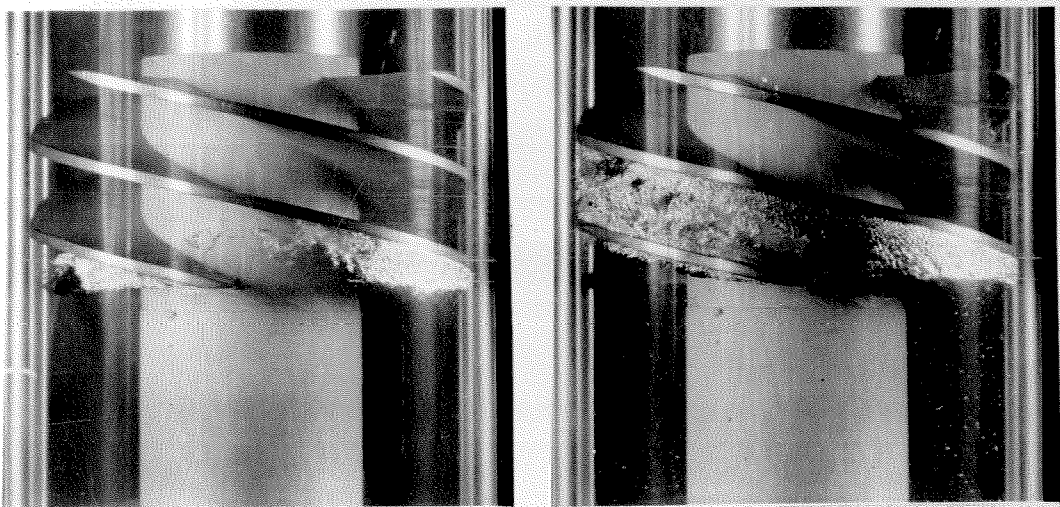


$K = 0.214$

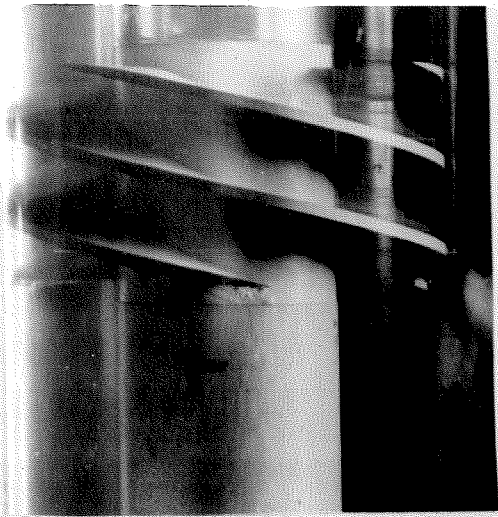


$K = 0.078$

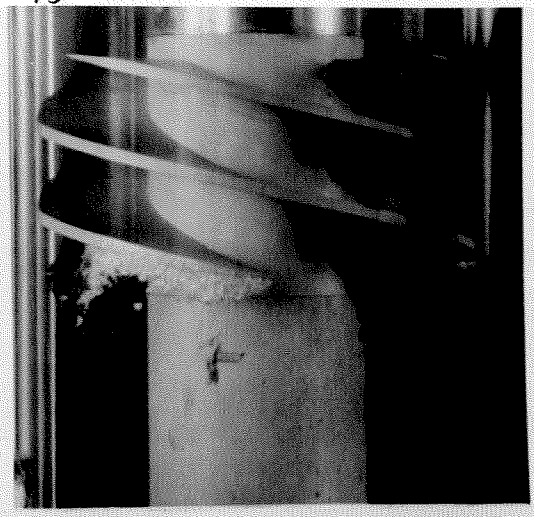
FIG. 23 CAVITATION DEVELOPMENT, IMPELLER ONE
 $\phi = 0.12$, RPM 6000



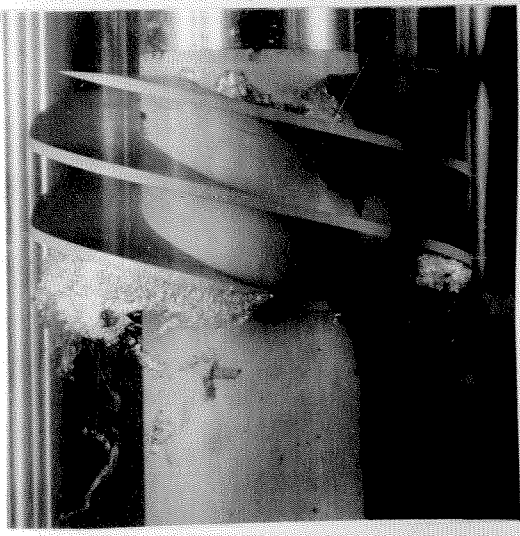
$K = 0.136$ $K = 0.074$
FIG. 24 CAVITATION DEVELOPMENT, IMPELLER ONE
 $\phi = 0.14$, RPM 6000



K = 0.768



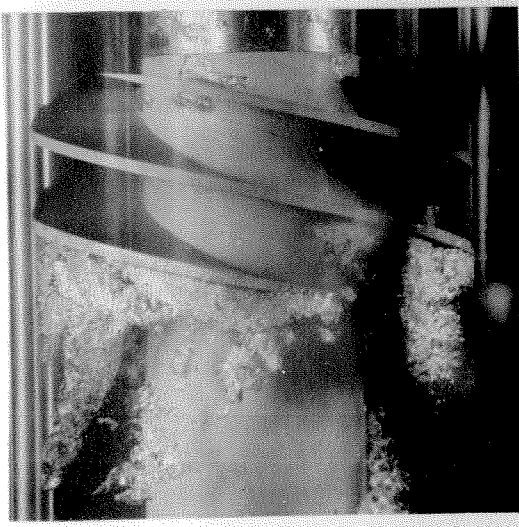
K = 0.245



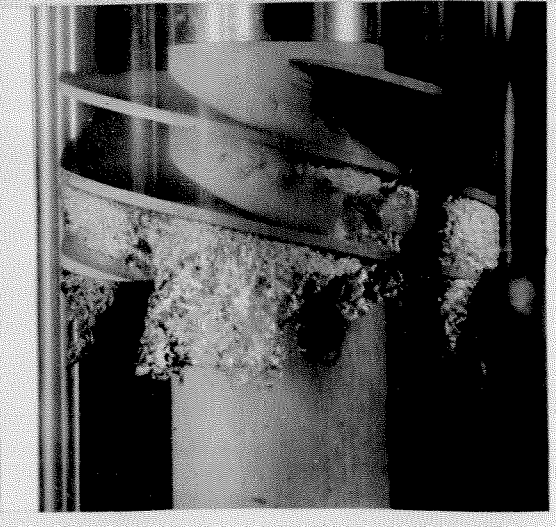
K = 0.146



K = 0.125

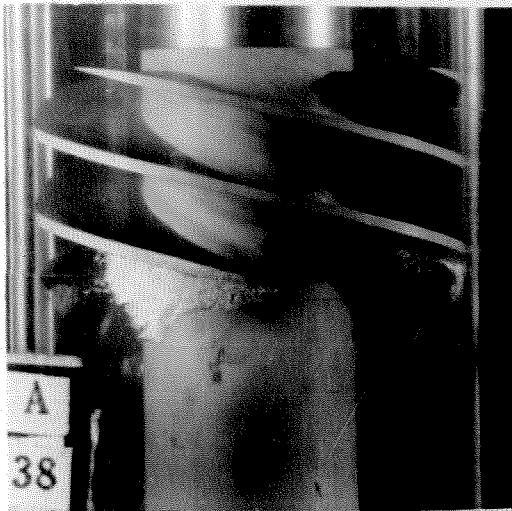


K = 0.096

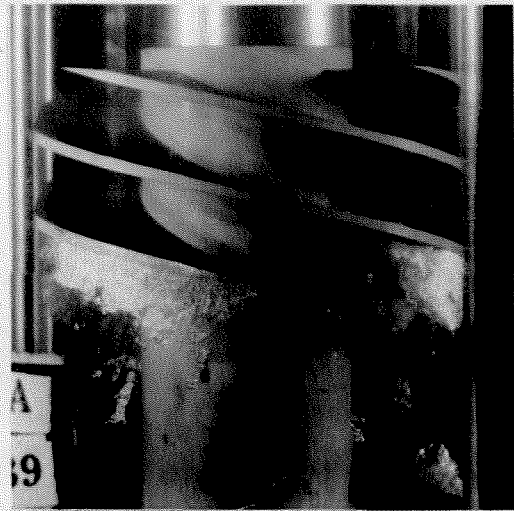


K = 0.071

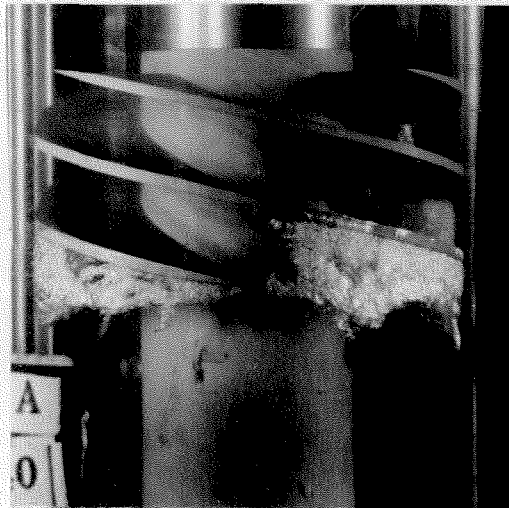
FIG. 25 CAVITATION DEVELOPMENT, IMPELLER TWO
 $\Phi = 0.08$, RPM 6000



$K = 0.247$



$K = 0.081$

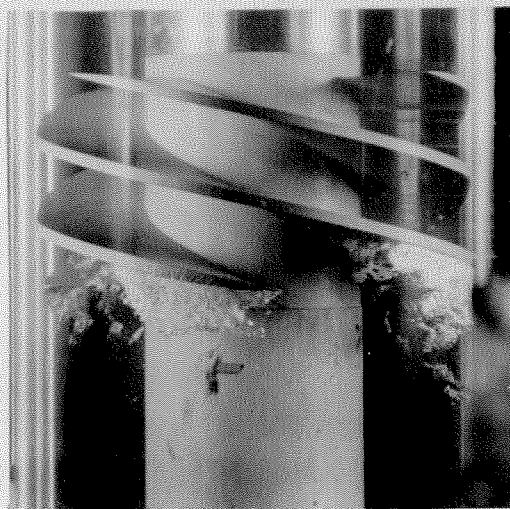


$K = 0.051$

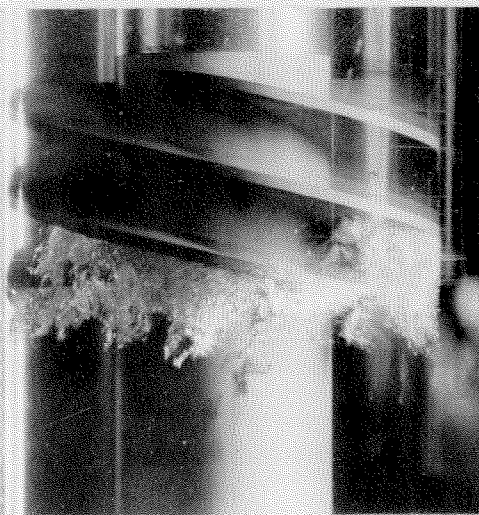
FIG. 26 CAVITATION DEVELOPMENT, IMPELLER TWO
 $\phi = 0.08$, RPM 9000



$K = 0.340$

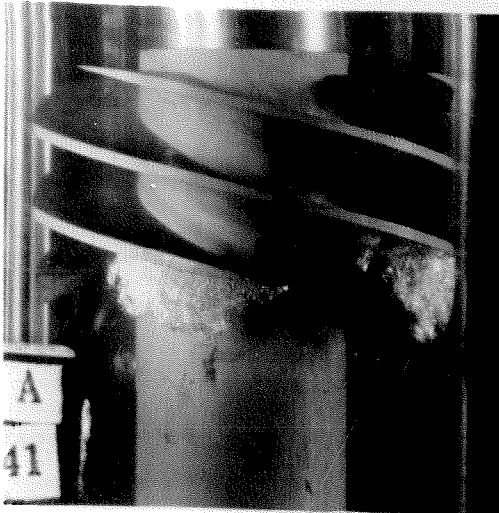


$K = 0.141$

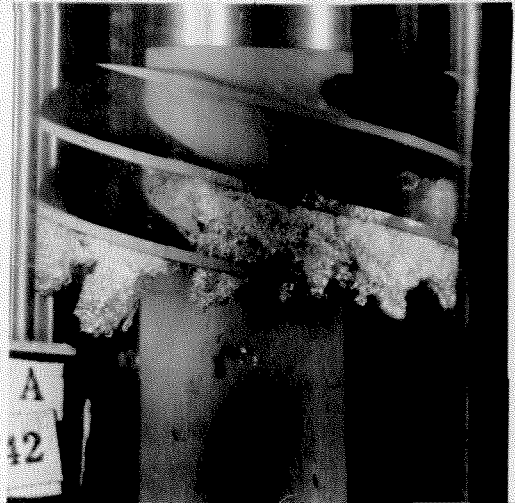


$K = 0.066$

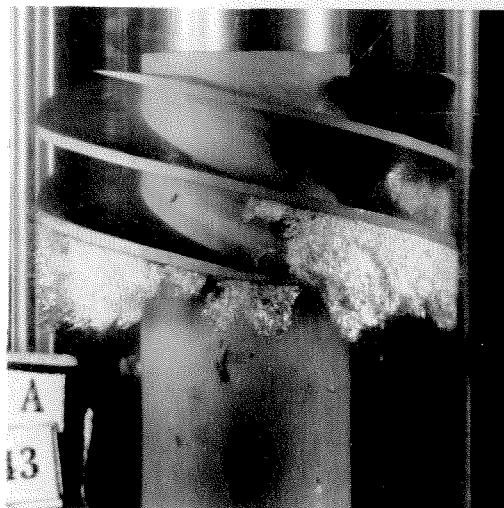
FIG. 27 CAVITATION DEVELOPMENT, IMPELLER TWO
 $\phi = 0.10$, RPM 6000



$K = 0.166$

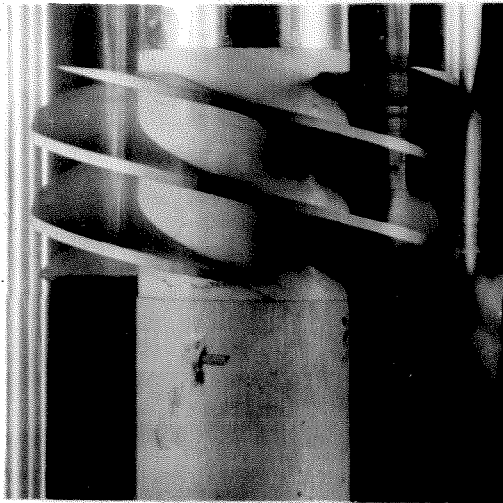


$K = 0.056$



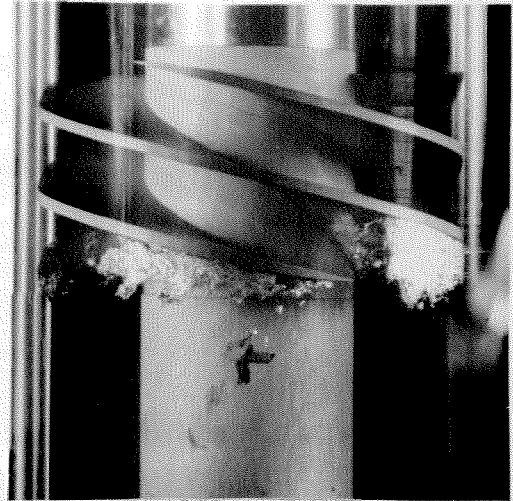
$K = 0.029$

FIG. 28 CAVITATION DEVELOPMENT, IMPELLER TWO
 $\phi \approx 0.10$, RPM 9000

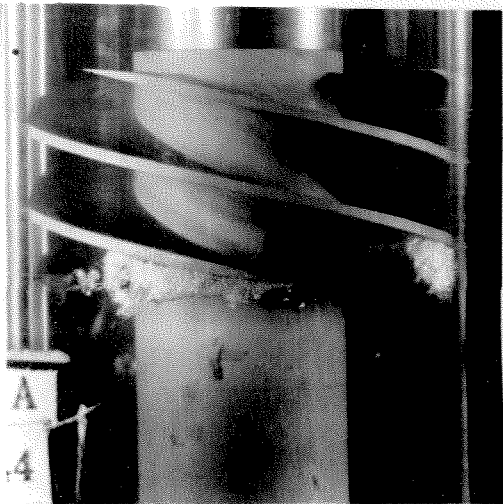


$K = 0.381$

RPM 6000

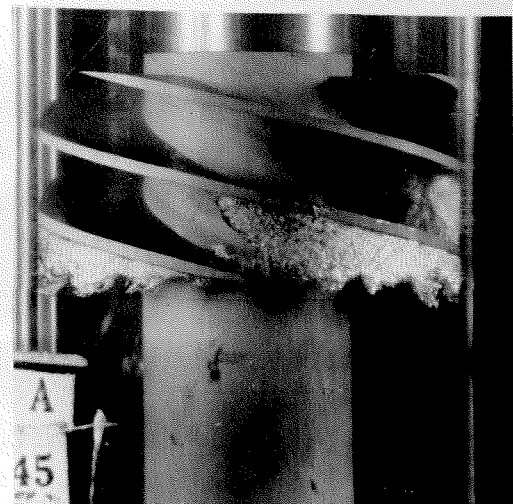


$K = 0.087$



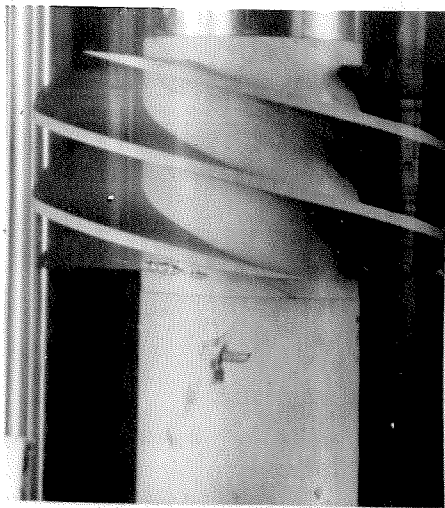
$K = 0.160$

RPM 9000



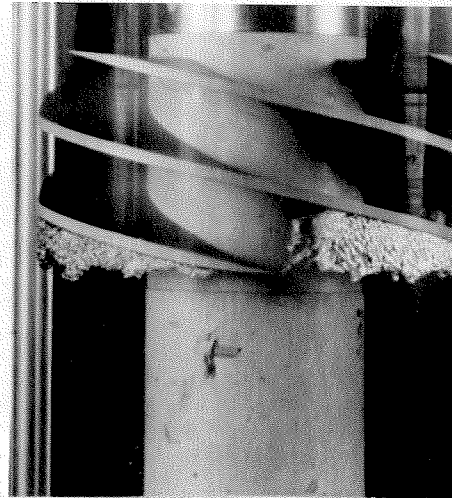
$K = 0.034$

FIG. 29 CAVITATION DEVELOPMENT, IMPELLER TWO
 $\phi = 0.12$



K = 0.171

RPM 6000

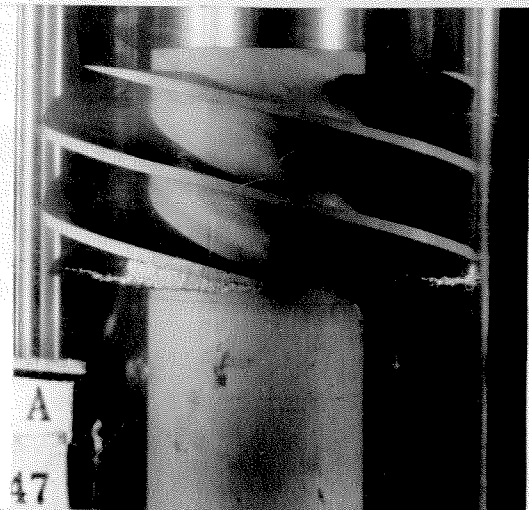


K = 0.052

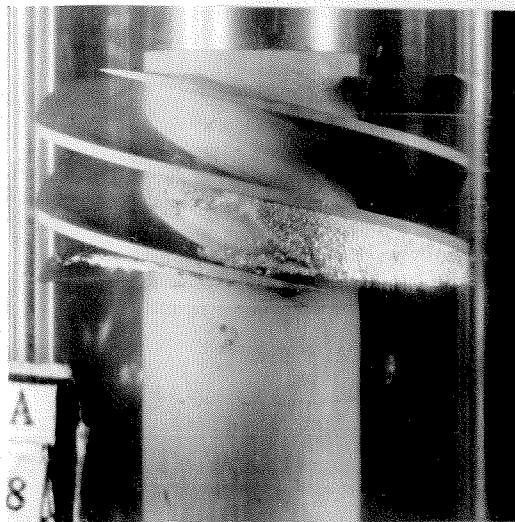


K = 0.237

RPM 9000

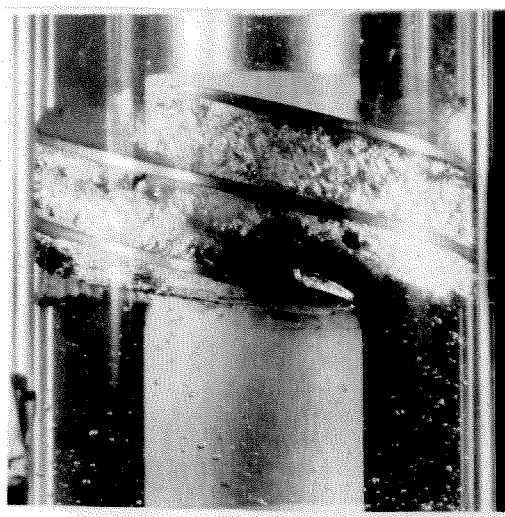


K = 0.155

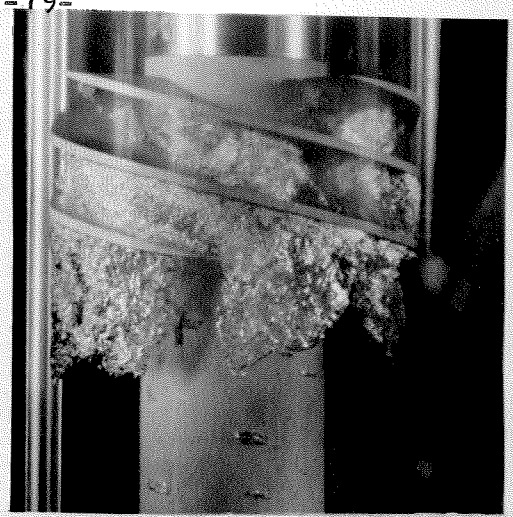


K = 0.059 RPM 9000

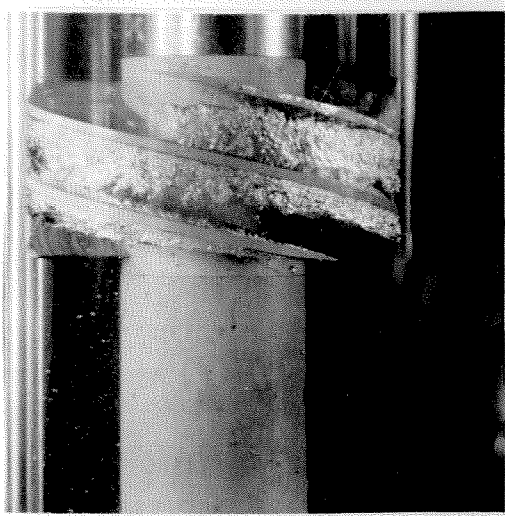
FIG. 30 CAVITATION DEVELOPMENT, IMPELLER TWO
 $\phi = 0.14$



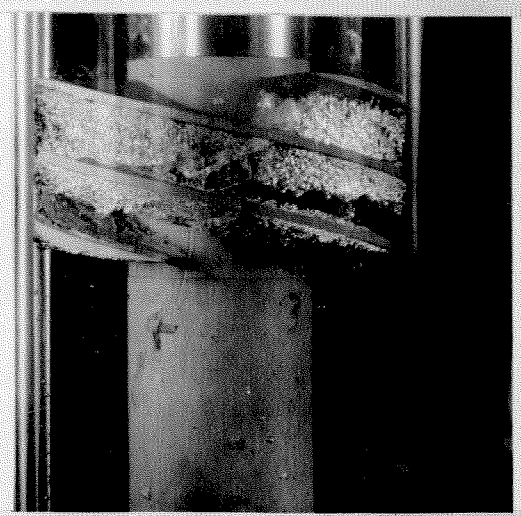
$K = 0.033$



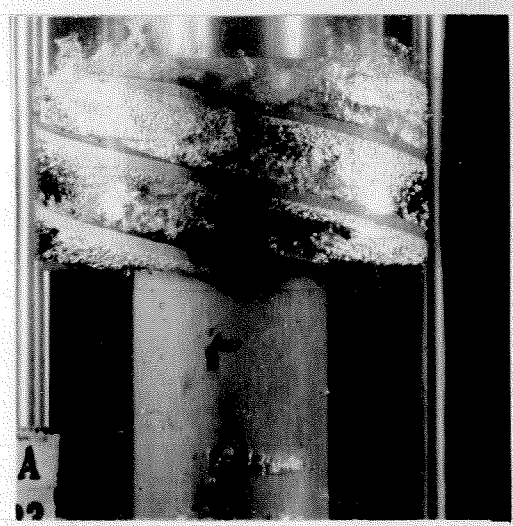
$K = 0.029$



$K = 0.030$



$K = 0.031$



$K = 0.012$

FIG. 31 TYPICAL CAVITATION BREAKDOWN OF THE IMPELLER.